$CD39^+$ tissue-resident memory $CD8^+$ T cells mediate anti-tumor immunity in breast cancer

Jee Ye Kim

Department of Medicine

The Graduate School, Yonsei University

$CD39^+$ tissue-resident memory $CD8^+$ T cells mediate anti-tumor immunity in breast cancer

Directed by Professor Seung Il Kim

The Doctoral Dissertation submitted
to the Department of Medicine, the Graduate School of
Yonsei University in partial fulfillment of the requirements for
the degree of Doctor of Philosophy in Medical Science

Jee Ye Kim

December 2022

This certifies that the Doctoral Dissertation of
Jee Ye Kim is approved.

Thesis Supervisor : Seung Il Kim

Thesis Committee Member#1 : Soonmyoung Paik

Thesis Committee Member#2 : Eui-chol Shin

Thesis Committee Member#3: Joo Hyuk Sohn

Thesis Committee Member#4: Hyung Seok Park

The Graduate School
Yonsei University

December 2022

ACKNOWLEDGEMENTS

I would like to express my deepest gratitude to my supervisor, Dr. Seung Il Kim. He has always been at my side guiding me through not only degree but also throughout my career.

I would like to thank Dr. Soonmyung Paik and Dr. Eui-chol Shin for their guidance and advice to research.

I would also like to thank my thesis committee, Dr. Joo Hyuk Sohn, Dr. Hyung Seok Park for thoughtful and detailed feedback.

I express my deepest gratitude to my loving husband, Jeong Hoon Ryou, and my most beloved daughter, Jay, who are indeed the greatest joy of my everyday life.

At last, I dedicate this thesis to my loving parents whom I respect the most in every aspect of life and who have been more than fully supportive throughout my life to this day.

December, 2022

Jee Ye Kim

<TABLE OF CONTENTS>

LIST OF FIGURES

ABSTRACT

CD39+ tissue-resident memory CD8+ T cells mediate anti-tumor immunity in breast cancer

Jee Ye Kim

Department of Medicine
The Graduate School, Yonsei University

(Directed by Professor Seung Il Kim)

Despite being a standard treatment option in breast cancer, immune checkpoint inhibitors currently show efficacy for only a subset of patients. To gain a better understanding of the anti-tumor immune response, we examined the heterogeneity of $CD8^+$ T cells in tumors, metastatic lymph nodes (mLNs), and peripheral blood from early breast cancer patients (n=131). Among tissue-resident memory $CD8^+$ T (TRM) cells, including virus- and tumor-specific $CD8^+$ T cells, CD39 expression was observed in a tumor-specific and exhausted subpopulation in both tumors and mLNs. $CD39^+$ TRM cell clonotypes overlapped with clonotypes of other $CD8^+$ T-cell subpopulations both in and across different compartments, implying that $CD39^+$ TRM cells are clonally connected to systemic anti-tumor immunity. $CD39^+$ TRM cell enrichment was heterogenous among molecular subtypes, which is associated with the different role of anti-tumor immune responses in each subtype. In vitro blockade of PD-1 and/or CTLA-4 effectively restored proliferation of $CD39^+$ TRM cells and enhanced cytokine production by $CD8^+$ T cells from tumors or mLNs, particularly in the presence of $CD39^+$ TRM enrichment, suggesting that $CD39^+$ TRM cells have a capacity for functional restoration upon ICI treatment.

Key words : breast cancer, $CD39^+$ Tissue-resident memory $CD8^+$ T cell, anti-tumor

immunity

CD39$^+$ tissue-resident memory CD8$^+$ T cells mediate anti-tumor immunity in breast cancer

Jee Ye Kim

Department of Medicine
The Graduate School, Yonsei University

(Directed by Professor Seung Il Kim)

I. INTRODUCTION

Immune checkpoint inhibitors (ICIs), including PD-1 and PD-L1 blockers, have demonstrated clinical efficacy in patients with advanced or metastatic breast cancer, especially in those with the triple negative breast cancer (TNBC) subtype(1, 2). In addition, the combination of ICIs with neoadjuvant chemotherapy leads to improved event-free survival and an increased pathological complete response (PCR) rate in TNBC, suggesting that neoadjuvant ICIs are a promising treatment option for early breast cancer patients(3-5). However, the treatment response to ICIs is low in patients with non-TNBC subtypes, which account of >80% of breast cancers(6-8), and the underlying mechanisms remain to be elucidated. In addition, the clinical value of immunological markers, including tissue expression of PD-L1 or the abundance of tumor-infiltrating lymphocytes (TILs), has not been clearly defined for predicting ICI treatment responses, indicating that our current knowledge of anti-tumor immune responses is limited in breast cancer.

Despite being initially considered as poorly immunogenic, breast cancer is an immunologically heterogeneous disease depending on the molecular subtype(9). Higher numbers of TILs have been observed in human epithelial growth factor receptor 2-positive (HER-2$^+$) or TNBC subtypes compared to hormone receptor-positive/HER-2-negative (HR$^+$/HER-2$^-$) subtypes(10, 11). Moreover, the abundance of TILs, especially CD8$^+$ TILs, has been shown to have a positive prognostic value only in patients with HER-2$^+$ or TNBC

subtypes(12-15), indicating heterogeneous roles of TILs among molecular subtypes of breast cancer.

Accumulating evidence implies heterogeneity among $CD8^+$ TILs in human cancers, especially in terms of antigen specificity. Low and variable tumor reactivity of the intra-tumoral T-cell receptor (TCR) repertoire has been reported in high-grade ovarian cancer (OVC) and microsatellite stable colorectal cancer (CRC)(16). Instead, tumor-nonspecific bystander $CD8^+$ T cells, including viral antigen-specific $CD8^+$ T cells, are abundant in tumor infiltrates from non-small-cell lung carcinoma (NSCLC) and CRC(17). In previous studies of OVC and NSCLC, $CD8^+$ TILs with phenotypes of tissue-resident memory $CD8^+$ T (T_{RM}) cells, which typically express CD69 and CD103, exhibited more tumor-specific features(18, 19). In breast cancer, previous studies have reported that $CD103^+CD8^+$ TILs are spatially located adjacent to tumor cells and associated with improved prognosis(20, 21). However, no study has comprehensively evaluated the heterogeneity of $CD8^+$ TILs in the context of tumor-specificity and its relationship with the anti-tumor immune response in breast cancer.

Previous studies have proposed CD39 as a marker for tumor antigen specificity(17, 22-25) or exhaustion(26), especially terminal exhaustion(27, 28). Although these concepts are related, their implications in the anti-tumor immune response can be interpreted differently. Enrichment of $CD39^+CD8^+$ TILs has shown a disparate prognostic significance(22, 23, 29) and different predictive abilities for the response to immune checkpoint blockade(30, 31) depending on the type of cancer. In this context, it is meaningful to characterize the phenotypes and functionalities of $CD39^+CD8^+$ T cells in depth and to investigate their significance on prognosis and ICI treatment in breast cancer.

In the current study, we examined the heterogeneity of $CD8^+$ T cells obtained from different compartments, including primary tumors, metastatic lymph nodes (mLNs), and peripheral blood, by recruiting multi-center cohorts of early breast cancer patients who underwent curative-aimed surgery.

II. MATERIALS AND METHODS

1. Characteristics of study patients

Clinical samples were prospectively obtained from 131 patients with early breast cancer who underwent surgical resection for curative aim between March 2015 and December 2020 at Severance Hospital, Gangnam Severance Hospital, Seoul St. Mary Hospital, and Daejeon St. Mary Hospital. All patients were given sufficient information on the study protocol and provided written informed consent. This study was approved by the Institutional Review Board of Severance Hospital (IRB Number: 4-2014-0054), Gangnam Severance Hospital (IRB Number: 3-2015-0342), Seoul St. Mary Hospital (IRB Number: KC18TEDI0854), and Daejeon St. Mary Hospital (IRB Number: DC18TESI0068).

2. Sample preparation

Adjacent normal and tumor breast tissue and LNs for which metastasis was confirmed by intraoperative frozen section examination were collected from patients. We also collected peripheral venous blood from each patient in sodium-EDTA tubes. Peripheral blood mononuclear cells (PBMCs) were isolated from peripheral venous blood by density gradient centrifugation using lymphocyte separation medium (Corning). Normal breast tissue, tumor breast tissue, and mLNs were mechanically divided into segments using the gentleMACS Dissociator and MACS C-tubes (Miltenyi Biotec), and enzymatically dissociated into single-cell suspensions using the Tumor Dissociation Kit (Miltenyi Biotec) according to the manufacturer's instructions. Dissociated single-cell suspensions were dispersed through a 70-μm filter. Isolated PBMCs and single-cell suspensions were cryopreserved in fetal bovine serum (FBS; Corning) with 10% dimethyl sulfoxide (Sigma Aldrich) and stored in liquid nitrogen at -80°C. Cryopreserved samples were thawed in a 37°C water bath and DNase (Thermo Fisher Scientific) added for 5 minutes at room temperature. Cells were washed with RPMI 1640 (Corning) $^{+}$ 10% FBS $^{+}$ 1% penicillin and streptomycin. After washing, cells were resuspended in appropriate medium for further

experiments.

3. Flow cytometry and data analyses

After thawing, dead cells were gated out using the LIVE/DEAD fixable dead cell stain kit (Invitrogen). Cells were washed once by stain buffer (BD) and stained with fluorochrome-conjugated antibodies against surface protein for 30 minutes at 4°C, and then washed again. For intra-cellular staining, the cells were fixed and permeabilized with the Foxp3 staining buffer kit (Thermo Fisher Scientific) and stained with fluorochrome-conjugated antibodies against intracellular protein. The following monoclonal antibodies were used for multi-color flow cytometry : anti-hCD3 BV510 (clone UCHT1, cat# 563109, 1:100), anti-hCD3 APC (clone HIT3a, cat# 300312, 1:100), anti-hCD4 BV605 (clone RPA-T4, cat# 562358, 1:100), anti-hCD4 FITC (clone RPA-T4, cat# 555346, 1:100), anti-hCD4 PerCP™Cy5.5 (clone RPA-T4, cat# 560650, 1:100), anti-hCD8 APC-Cy7 (clone SK1, cat# 560179, 1:100), anti-hCD8 BV605 (clone SK1, cat# 564116, 1:100), anti-hCD8 BV711 (clone RPA-T8, cat# 563677, 1:100), anti-hCD8 FITC (clone RPA-T8, cat# 301050, 1:100), anti-hCD14 PE-CF594 (clone MφP9, cat# 562335, 1:100), anti-hCD14 PE-Cy7 (clone MφP9, cat# 562698, 1:100), anti-hCD19 PE-CF594 (clone HIB19, cat# 562294, 1:100), anti-hCD69 PE-Cy7 (clone FN50, cat# 557745, 1:100), anti-hCD69 PerCP™Cy5.5 (clone FN50, cat# 560738, 1:100), anti-hCD137 APC (clone 4B4-1, cat# 550890, 1:100), anti-hCD137 PE (clone 4B4-1, cat# 309804, 1:100), anti-hIFN-γ PE-Cy7 (clone 4S.B3, cat# 557844, 1:100), anti-hIL-2 APC (clone MQ1-17H12, cat# 554567, 1:100), anti-hKi-67 BV786 (clone B56, cat# 563756, 1:100), anti-hKi-67 BV711 (clone Ki-67, cat# 350516, 1:100), anti-hTNF AF700 (clone Mab11, cat# 557996, 1:100), anti-hCCR7 PerCP™Cy5.5 (clone G043H7, cat# 353220, 1:100), anti-hCD45RA APC-Cy7 (clone HI100, cat# 304128, 1:100), anti-hPD-1 BV421 (clone EH12.2H7, cat# 329920, 1:100), anti-hCD103 BB515 (clone Ber-ACT8, cat# 564578, 1:100), anti-hCD56 BV786 (clone NCAM16.2, cat# 564058, 1:100), anti-hCD11b BV510 (clone ICRF44, cat# 563088, 1:100), anti-hCD11c FITC (clone B-ly6, cat# 561355, 1:100), anti-hCD15 BV650 (clone HI98, cat# 564232, 1:100), anti-hCD39

BB515 (clone Tü66, cat# 565469, 1:100), anti-hCD39 BV711 (clone Tü66, cat# 563680, 1:100), anti-hCD45 AF700 (clone HI30, cat# 560566, 1:100), anti-hTIM-3 BV785™ (clone F38-2E2, cat# 345031, 1:100), anti-hHLA-DR BV785™ (clone L243, cat# 307642, 1:100), anti-hCTLA-4 PerCP-eFluor 710 (clone 14D3, cat# 46-1529-42, 1:100), anti-hTOX PE (clone TXRX10, cat# 12-6502-82, 1:100), anti-hEomes PE-Cy7 (clone WD1928, cat# 25-4877-42, 1:100), and anti-hT-bet APC (clone eBio4B10, cat# 17-5825-82, 1:100) from BD Biosciences, BioLegend, or Invitrogen. Flow cytometry analyses were performed on an LSR II instrument using FACSDiva software (BD Biosciences). The data were analyzed by FlowJo software (Treestar).

4. Multimer staining

After thawing, cells were incubated with dasatinib (50 nM, Sigma-Aldrich) for 15 minutes at 37°C, and then stained with fluorochrome-conjugated HLA-A*0201 dextramers for NY-ESO-$1_{157-165}$ (SLLMWITQV; Immudex) or HLA-A*0201 pentamers for CMV $pp65_{495-503}$ (NLVPMVATV; Proimmune) or Flu $M1_{58-66}$ (GILGFVFTL; Proimmune) for 15 minutes at room temperature. After washing once by stain buffer, the cells were incubated with purified anti-phycoerythrin (PE; Biolegend), purified anti-fluorescein (FITC; Biolegend), or anti-allophycocyanin (APC; Biolegend) antibodies for 15 minutes at room temperature, and then washed again. Surface proteins or intracellular proteins were stained by fluorochrome-conjugated antibodies as above and flow cytometry analyses were performed.

5. RNA-sequencing and data analyses

After thawing, single-cell suspensions of tumors were enriched using CD8 Microbeads and manual MACS magnetic separators (Miltenyi Biotec) following the manufacturer's instructions. Enriched tumor-infiltrating $CD8^+$ T cells were sorted into $CD103^-CD39^-$, $CD103^+CD39^-$, and $CD103^+CD39^+$ subpopulations using a FACSAria II cell sorter (BD Biosciences). The SMART-Seq® v4 Ultra® Low Input RNA kit for sequencing (Takara Bio USA) was used to extract total RNA, to synthesize cDNA from mRNA, to amplify

cDNA, and to construct a library following the manufacturer's instructions. The amplified cDNA quality was validated using Agilent high sensitivity DNA kit and the Agilent 2100 bioanalyzer. Libraries were pooled and high-throughput sequencing was performed by paired-end 100 bp x 2 running scale using the Hiseq 2500 (Illumina). Raw reads were trimmed using Trimmomatic v.0.38, and the trimmed reads were aligned to the human genome using HISAT2 v.2.1.0 with default parameters. The aligned reads were used to assemble transcripts and counted using StringTie v.1.3.4d. Read counts were normalized by effective library size and differentially expressed genes (DEGs) determined using R package DESeq2(61). DEG analysis was performed using a generalized linear model with the Wald statistical test. DEGs were defined by a false discovery rate (FDR) <0.01 and a $\log_2$fold change >1. Clustering of DEGs was performed with unsupervised hierarchical clustering primarily to segregate up-regulated and down-regulated genes. Gene ontology (GO) biological pathway analysis was conducted with the R package clusterProfiler using up-regulated DEGs in $CD39^+$ T_{RM} cells compared to $CD39^-$ T_{RM} cells, with a Bonferroni correction and an adjusted p value of 0.05.

6. Gene set enrichment analysis and survival analysis using an extra dataset

GSEA was used to assess the enrichment of specific gene sets extracted from previous studies. Up-regulated genes in the $CD8^+$ T_{RM}-like cluster or $CD8^+$ T_{EM}-like cluster were obtained from the previous single-cell RNA-seq analysis using breast tumor samples (data available at https://doi.org/10.5281/zenodo.1169607 and https://doi.org/10.5281/zenodo.1170580)(20). Up-regulated genes in exhausted $CD8^+$ T cells versus memory $CD8^+$ T cells were obtained from the previous study using the mouse lymphocytic choriomeningitis virus (LCMV) model (data available at https://www.ncbi.nlm.nih.gov/geo/query/acc.cgi?acc=gse9650)(38). Up-regulated genes in expanding versus non-expanding $CD8^+$ T cells upon neoadjuvant anti-PD-1 treatment were obtained from the previous single-cell RNA-seq analysis using pretreatment tumor samples from a clinical trial of human breast cancer (data available at https://ega-

archive.org/studies/EGAS00001004809)(5). GSEA was performed using the R package clusterProfiler. The single-cell RNA-seq data for T cells in tumors were obtained from a clinical trial (IMPASSION131 trial) of 22 patients with TNBC who underwent anti-PD-L1 treatment (data available at https://www.ncbi.nlm.nih.gov/geo/query/acc.cgi?acc=GSE169246)(45). Enrichment scores for our $CD39^+$ T_{RM} gene signature were calculated in each subpopulation of T cells using the AddModuleScore function of the R package Seurat.

To assess the expression and prognostic value of the $CD39^+$ T_{RM} signature, we referred to the survival analysis pipeline in the previous paper(20). Gene expression and survival data from the METABRIC dataset(43), TCGA dataset, and GSE46141(44) (data available at https://www.ncbi.nlm.nih.gov/geo/query/acc.cgi?acc=GSE46141) were accessed through cBioPortal(62) (data available at https://www.cbioportal.org/) or Gene Expression Omnibus(63) (data available at https://www.ncbi.nlm.nih.gov/geo/) and analyzed in R. Breast cancer samples were classified by molecular subtype based on the expression of hormone receptors and HER-2 receptor. Gene expression from the METABRIC dataset was assessed using Kaplan–Meier survival curves generated by stratifying cases in a 50:50 split based on the ranked signature expression, which was determined using the 'sig.score' function in R package genefu.

7. TCR sequencing and data analyses

After thawing, PBMCs and single-cell suspensions of tumors and LNs were enriched using CD8 Microbeads and manual MACS magnetic separators (Miltenyi Biotec) following the manufacturer's instructions. Enriched $CD8^+$ T cells were sorted into various $CD8^+$ T-cell subpopulations using a FACSAria II cell sorter (BD Biosciences). $CD8^+$ T cells were primarily sorted into $CCR7^+CD45RA^+$ T_N, $CCR7^+CD45RA^-$ T_{CM}, $CCR7^-CD45RA^-$ T_{EM}, and $CCR7^-CD45RA^+$ T_{EMRA} cells. In tumors and mLNs, $CCR7^-CD45RA^-$ T_{EM} cells were further sorted into $CD103^-CD39^-$, $CD103^+CD39^-$, and $CD103^+CD39^+$ subpopulations. After being sorted by a FACSAria II cell sorter, diverse $CD8^+$ T-cell subpopulations from

tumors, mLNs, and blood were constructed into libraries. Sequencing libraries were prepared using the SMARTer Human TCR a/b Profiling Kit (Takara Bio USA). Briefly, after synthesizing cDNA from extracted mRNA and amplifying the synthesized cDNA, we constructed a library following the manufacturer's instructions. The quality of the amplified cDNA was validated using an Agilent high sensitivity DNA kit and the Agilent 2100 bioanalyzer. Illumina HT indexes were used as indexing adapters. Resulting TCRα/β libraries were pooled and sequenced on an Illumina MiSeq system (paired-end 150 bp). Raw reads of sequence data were aligned and subsequently assembled by MiXCR with default parameters(64). Extracted TCR-alpha or -beta CDR3 repertories were analyzed in R version 4.1.0. Detailed information on TCR sequencing statistics is given in Table S1 and Fig. S3A. A distinct CDR3 nucleic-acid sequence of the TCR-beta chain was considered as a clonotype of $CD8^+$ T cells in this study. The population diversity of the T-cell repertoire was quantified using the Shannon entropy index(65). The degree of clonal overlap between two populations was calculated using the Morisita-horn overlap index in R package Immunarch(66, 67).

8. Proliferation assays

After thawing, single-cell suspensions of tumors and LNs rested overnight. We then stained the single-cell suspensions using the Cell Trace Violet (CTV) cell proliferation kit (Thermo Fisher Scientific) according to the manufacturer's instructions to assess cellular proliferation. Stained cells were seeded in round-bottom 96-well plates (0.2M/well) and stimulated ex vivo with anti-CD3 antibody (10 ng/ml; clone OKT3; eBioscience). Cells were cultured in RPMI 1640 (Corning) containing 10% FBS and 1% penicillin-streptomycin. For the T-cell restoration assay, anti-PD-1 antibody (10 μg/ml, Biolegend) and/or anti-CTLA-4 antibody (10 μg/ml, Biolegend) was added. For the control well, mouse IgG1 isotype control antibody (10 μg/ml, Biolegend) was added. After 108 hours, the cells were harvested and the dilution of CTV measured by flow cytometry. The mitotic index was calculated by dividing the total number of mitotic events by the absolute number

of precursor cells.

For tumor-specific stimulation, tumor cells were depleted from single-cell suspensions of tumors using CD326 (EPCAM) Microbeads and manual MACS magnetic separators (Miltenyi Biotec). $CD8^+$ TILs were then isolated from tumor-depleted single-cell suspensions using CD8 Microbeads and manual MACS magnetic separators (Miltenyi Biotec), and remnant single-cell suspensions were irradiated for use as feeder cells. Isolated $CD8^+$ TILs were stained with CTV, seeded in 96-well plates (0.1M - 0.2M/well), and stimulated with NY-ESO-1 OLPs (1 μg/ml/peptide, JPT) or autologous tumor cells (0.1M - 0.2M/well) in the presence of irradiated feeder cells (0.1 - 0.2M/well). Cells were cultured in RPMI 1640 (Corning) containing 10% FBS and 1% penicillin-streptomycin. For T-cell restoration assays, anti-PD-1 antibody and/or anti-CTLA-4 antibody was added. For the control well, mouse IgG1 isotype control antibody (10 μg/ml, Biolegend) was added. After incubation for 144 hours, $CD8^+$ TILs were harvested and proliferation measured as indicated above.

9. Intracellular cytokine staining

For cytokine production assays, single-cell suspensions of tumors and LNs that had rested overnight or sorted subpopulations of $CD8^+$ TILs ($CD39^+CD103^+$, $CD39^-CD103^+$, and $CD39^-CD103^-$) were seeded in 96-well plates (0.2M/well) and stimulated ex vivo with anti-CD3 antibody (10 μg/ml; clone OKT3; eBioscience). Cells were cultured with Brefeldin A (1:1000, BD Biosciences) and Monensin (1:1000, BD Biosciences) in RPMI 1640 (Corning) containing 10% FBS and 1% penicillin-streptomycin. After 6 hours, cells were harvested and stained with fluorochrome-conjugated antibodies against surface markers. After being fixed and permeabilized, cells were stained with fluorochrome-conjugated anti-IFN-γ, anti-TNF-α , or IL-2 antibodies and cytokine production measured by flow cytometry.

For T-cell restoration assays, single-cell suspensions of tumors and LNs were thawed and rested overnight. The single-cell suspensions were then seeded in 96-well plates (0.2M/well) and stimulated ex vivo with anti-CD3 antibody (10 μg/ml; clone OKT3; eBioscience).

Anti-PD-1 antibody (10 μg/ml, Biolegend) and/or anti-CTLA-4 antibody (10 μg/ml, Biolegend) was added, and mouse IgG1 isotype control antibody (10 μg/ml, Biolegend) was added to a control well. After 24 hours, cells were incubated with Brefeldin A (1:1000, BD Biosciences) and Monensin (1:1000, BD Biosciences). After another 12 hours, cells were harvested and stained with fluorochrome-conjugated antibodies against surface markers. After being fixed and permeabilized, cells were stained with fluorochrome-conjugated anti-IFN-γ, anti-TNF-α, or IL-2 antibodies and cytokine production measured by flow cytometry.

10. Statistics and reproducibility

Categorical data are presented as frequencies with percentages. Continuous data are presented as means with standard deviations. The intergroup differences were analyzed using the unpaired Student's t-test or Mann-Whitney U-test depending on whether the data satisfied the assumption of a normal distribution. The paired Student's t-test or Wilcoxon signed-rank test were used to compare matched samples depending on whether the data satisfied the assumption of a normal distribution. One-way analysis of variance (ANOVA) was used to compare parametric data between multiple unpaired groups. Kaplan-Meier survival curves were analyzed by two-sided log-rank tests. All tests were two-sided. $P < 0.05$ was considered significant, and confidence intervals (CIs) were calculated at the 95^{th} percentile. For all statistical tests involving multiple comparisons, an FDR-adjusted $P < 0.05$ was considered significant. GraphPad Prism ver. 7 (GraphPad Software, La Jolla, Ca) or R (version 4.1.0) were used for statistical analyses and to present the analyzed data as graphs. In flow cytometry, if there were fewer than 100 events of gated subpopulations, data were excluded from the analyses. Otherwise no data was excluded from the analyses. No statistical method was used to predetermine sample sizes. Experiments were not randomized, and investigators were not blinded. Experiments did not include replicates, as all participants and their data are unique.

III. RESULTS

1. CD39 expression enriches a tumor-specific subpopulation of T_{RM} cells

We examined the composition of immune cells in peripheral blood and tumor tissues from patients with early breast cancer (n=131) using multi-color flow cytometry. Among live $CD45^+$ cells, T cells were the major immune cell subset in tumors. The percentage of $CD8^+$ T cells among T cells was significantly higher in tumors than in the peripheral blood). We examined TRM markers, such as CD69 and CD103, on $CD8^+$ T cells. The percentage of $CD69^+CD103^+$ TRM cells among $CD8^+$ T cells was significantly higher in tumors than the peripheral blood (Fig. 1). CD103 was co-expressed by a subpopulation of $CD69^+CD8^+$ T cells in tumors.

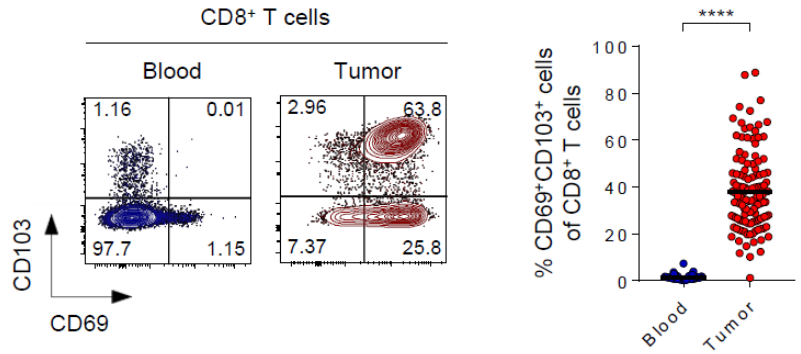

(a) (b)

Fig. 1. Representative flow cytometry plots of TRM marker expression (a) and frequencies of $CD69^+CD103^+$ cells among $CD8^+$ T cells (b) in blood (n = 122) and tumors (n = 131) from patients with breast cancer. Bars represent means. Two-sided unpaired Student′s t test.

We also examined the antigen-specificity of $CD8^+$ T cells. We detected virus-specific bystander $CD8^+$ T cells that are unrelated to tumor antigens using human leukocyte antigen

(HLA)-A*02 multimers loaded with human cytomegalovirus (HCMV) pp65495-503 or influenza A virus (IAV) M158-66 peptide (Fig. 2). Although the percentages of HCMV- or IAV-specific cells among $CD8^+$ T cells varied across patients, the percentage of IAV-specific cells among $CD8^+$ T cells was significantly increased in tumors compared to peripheral blood, but we found no difference in the percentage of HCMV-specific cells (Fig. 2). This difference could be explained by the fact that approximately half of IAV-specific cells were $CD69^+CD103^+$ TRM cells, whereas <10% of HCMV-specific cells were TRM cells.

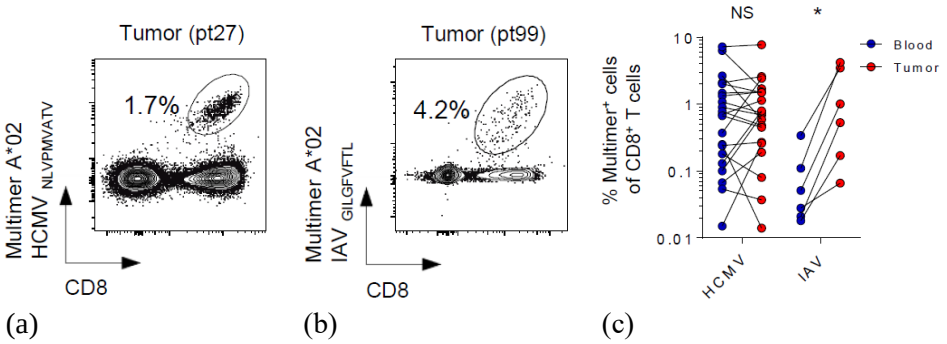

Fig. 2. (a, b) Representative flow cytometry plots showing ex vivo detection of HLA-A*02-multimer$^+$ $CD8^+$ T cells in two patients. pt, patient. a: HCMV-specific $CD8^+$ T cells. b: IAV-specific $CD8^+$ T cells. (c) Frequencies of HCMV-specific $CD8^+$ T cells (n = 21) or IAV-specific $CD8^+$ T cells (n = 6) identified by multimer staining in blood and tumors.

Next, we used an HLA-A*02 multimer loaded with NY-ESO-1157-165 peptide to detect tumor antigen-specific $CD8^+$ T cells. NY-ESO-1 is a cancer-testis antigen that is overexpressed across various types of tumors, including breast cancer, particularly the TNBC subtype (32, 33). NY-ESO-1-specific cells were only detected among $CD8^+$ TILs from patients with TNBC and were simultaneously detected in peripheral blood $CD8^+$ T cells from certain cases. $CD69^+CD103^+$ TRM cells were the dominant population in NY-ESO-1-specific $CD8^+$ TILs but were absent in NY-ESO-1-specific peripheral blood $CD8^+$

T cells (Fig. 3a, 3b). In addition, the percentage of $CD69^{+}CD103^{+}$ TRM cells was significantly increased among NY-ESO-1-specific $CD8^{+}$ TILs compared to total $CD8^{+}$ TILs (Fig. 3c), indicating that TRM cells are preferentially enriched in tumor antigen-specific $CD8^{+}$ TILs but also found among IAV-specific $CD8^{+}$ TILs. As CD103 was expressed exclusively by $CD69^{+}CD8^{+}$ cells, $CD103^{+}CD8^{+}$ T cells were regarded as TRM cells.

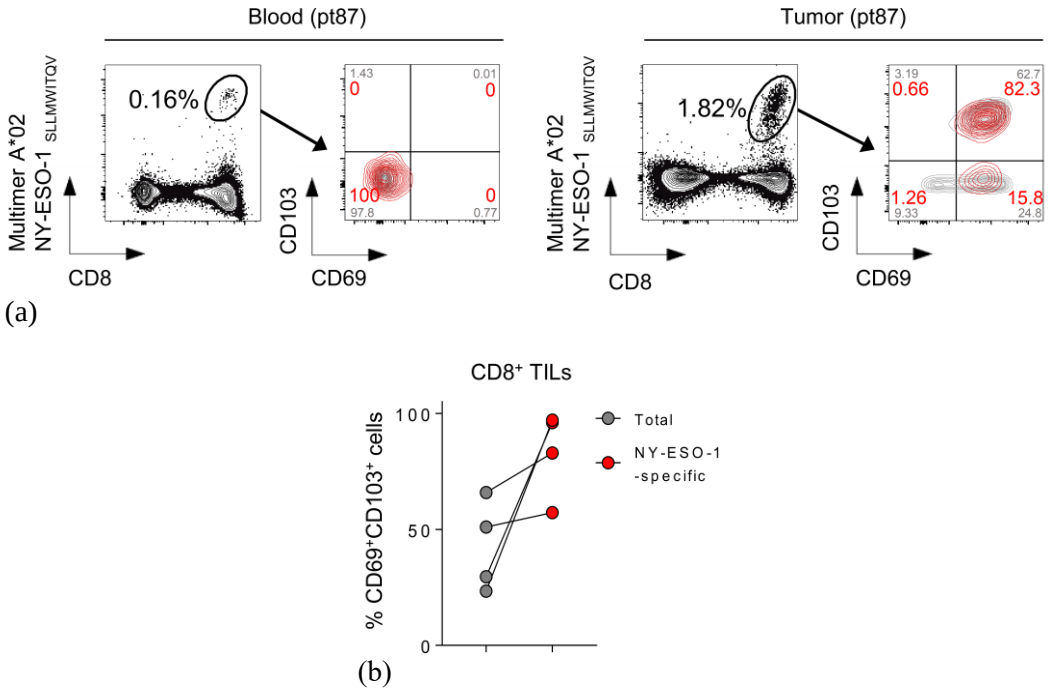

Fig. 3. Ex vivo detection of NY-ESO-1–specific $CD8^{+}$ T cells and their expression of TRM markers. Representative flow cytometry plots (a) and frequencies of $CD69^{+}CD103^{+}$ cells among NY-ESO-1–specific $CD8^{+}$ TILs or total $CD8^{+}$ TILs (b, n = 4). Numbers that are colored in red in gating plots indicate the percentages of gated subsets among NY-ESO-1–specific $CD8^{+}$ T cells. Numbers that are colored in gray in gating plots indicate the percentages of gated subsets among total $CD8^{+}$ T cells.

To better define tumor antigen-specific CD8$^+$ T cells, we stained CD39, which was previously reported to be a marker of tumor antigen-specific CD8$^+$ T cells in several types of cancers (17, 22-25). CD39 expression was restricted in CD103$^+$ TRM cells, and CD39$^+$CD103$^+$ TRM cells were observed only in NY-ESO-1-specific CD8$^+$ TILs, but not in IAV- or HCMV-specific CD8$^+$ TILs (Fig. 4). We also compared the expression of CD39 between CD8$^+$ T cells from tumor and tumor-adjacent normal tissues. Although the percentage of CD103$^+$ TRM cells among CD8$^+$ T cells was not different between tumor and normal tissues, the percentage of CD39$^+$CD103$^+$ TRM cells was significantly increased in tumor tissues compared to normal tissues (Fig.5). Taken together, these results indicate that CD39 expression enriches tumor antigen-specific TRM cells in breast cancer.

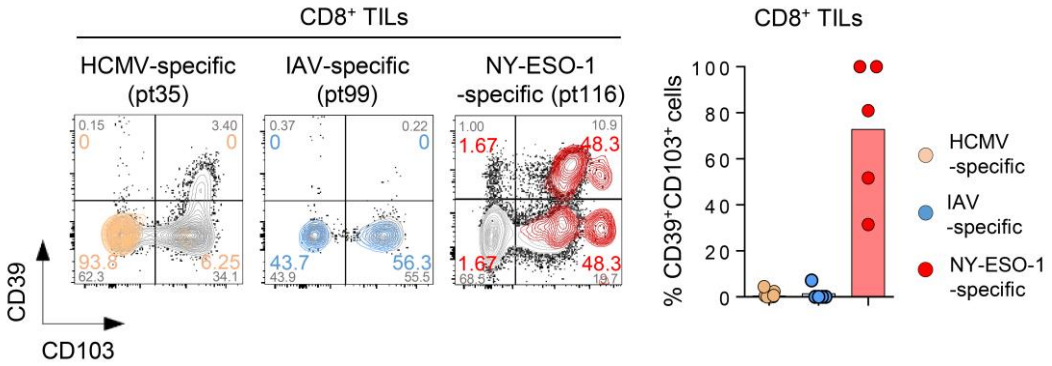

Fig. 4. Comparison of CD39 and CD103 expression among multimer$^+$ CD8$^+$ TILs. Representative flow cytometry plots (a). Frequencies of CD39$^+$CD103$^+$ cells among multimer$^+$ CD8$^+$ TILs (b): HCMV-specific (n = 21), IAV-specific (n = 5), and NY-ESO-1–specific (n = 5). Bars represent means.

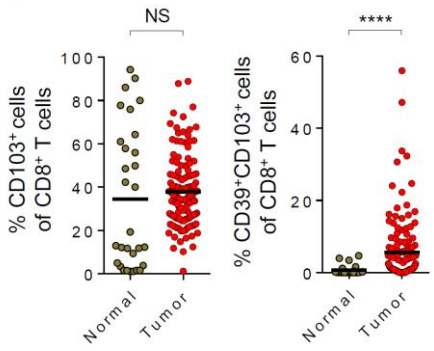

(a) (b)

Fig. 5. Frequencies of $CD103^+$ cells (a) and $CD39^+CD103^+$ cells (b) among $CD8^+$ T cells in normal tissues (n = 30) and tumors (n = 131). Two-sided unpaired Student′s t test. *P ≤ 0.05 and ****P ≤ 0.0001. NS, not significant.

2. $CD39^+$ T_{RM} cells are exhausted in both tumors and mLNs

To comprehensively investigate the transcriptomic characteristics of $CD39^+CD103^+$ T_{RM}, we sorted $CD8^+$ TILs into three subpopulations to perform bulk mRNA-seq: $CD39^+$ T_{RM} ($CD39^+CD103^+$), $CD39^-$ T_{RM} ($CD39^-CD103^+$), and non-T_{RM} ($CD39^-CD103^-$) cells. Gene clustering analysis showed that $CD39^+$ T_{RM} cells had distinct transcriptomic profiles compared to $CD39^-$ T_{RM} and non-T_{RM} cells (Fig. 6). $CD39^+$ T_{RM} cells highly expressed TOX, the gene encoding a DNA-binding factor that programs T-cell exhaustion(34-37), and immune checkpoint-related genes, including LAYN, CXCL13, HAVCR2, and TIGIT, compared to $CD39^-$ T_{RM} or non-T_{RM} cells. In addition, $CD39^+$ T_{RM} cells exhibited upregulation of genes related to effector functions, including GZMB and IFNG, and genes related to T-cell activation, including TNFRSF9, HLA-DRA, and HLA-DRB1. In contrast, $CD39^+$ T_{RM} cells exhibited downregulation of IL7R and CCR7, which are associated with naïve or central memory $CD8^+$ T cells compared to $CD39^-$ T_{RM} or non-T_{RM} cells. Gene

Ontology (GO) biological pathway analysis revealed cell activation features in CD39^{+} TRM cells compared to CD39^{-} TRM cells (Fig. 7).

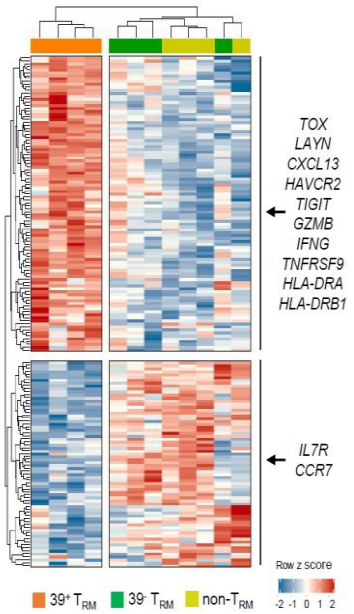

Fig. 6. Heat map comparing gene signatures derived from bulk RNA-seq and unsupervised clustering of the DEGs among three subpopulations of CD8^{+} T cells in tumors (HER-2^{+}, n = 2; TNBC, n = 2); CD39^{+} TRM cells (39^{+} TRM), CD39^{-} TRM cells (39^{-} TRM), and non-TRM cells (Non-TRM).

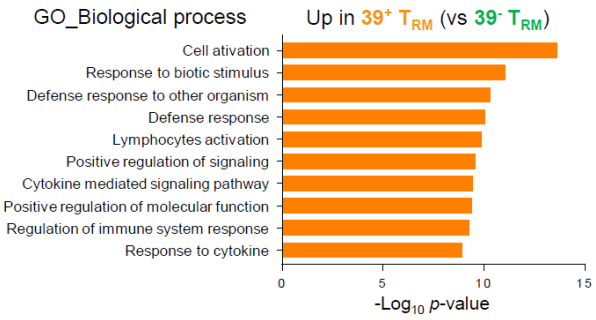

Fig. 7. Bar plots showing enrichment P values for the top 10 GO biological pathways in CD39^{+} TRM cells for up-regulated genes compared with CD39^{-} TRM cells.

We also performed gene set enrichment analysis (GSEA) using gene sets from recently identified $CD8^+$ T-cell clusters based on single-cell RNA-seq analysis in breast cancer(20). Interestingly, up-regulated genes in the T_{RM}-like cluster were enriched in $CD39^+$ T_{RM} cells compared to $CD39^-$ T_{RM} cells, but up-regulated genes in the effector memory T (T_{EM})-like cluster were enriched in $CD39^-$ T_{RM} cells compared to $CD39^+$ T_{RM} cells (Fig. 8a). GSEA also revealed that up-regulated genes in exhausted $CD8^+$ T cells from a model of chronic viral infection were enriched in $CD39^+$ T_{RM} cells compared to $CD39^-$ T_{RM} or non-T_{RM} cells(38) (Fig. 8b).

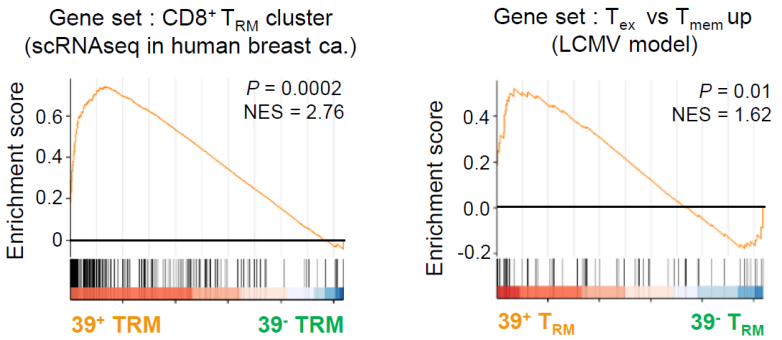

Fig. 8. GSEA of $CD8^+$ TRM cluster gene sets from previous scRNA-seq data for human breast cancer (20) (a) or up-regulated gene sets in exhausted T cells versus memory T cells from a mouse LCMV model (38) (b) in $CD39^+$ TRM and $CD39^-$ TRM cells. NES, normalized enrichment score.

Flow cytometric analysis of TILs confirmed the results of the transcriptomic analysis. The frequencies of PD-1^+ and PD-1^{bright} cells were significantly higher in $CD39^+$ T_{RM} cells than in $CD39^-$ T_{RM} and non-T_{RM} cells and were significantly higher in $CD39^-$ T_{RM} cells than in non-T_{RM} cells. The frequencies of TIM-3^+ and CTLA-4^+ cells were also significantly higher in $CD39^+$ T_{RM} cells than in $CD39^-$ T_{RM} and non-T_{RM} cells (Fig. 9). Moreover, the expression of TOX was significantly higher in $CD39^+$ T_{RM} cells than in $CD39^-$ T_{RM} or non-T_{RM} cells

(Fig. 10). Upon anti-CD3 stimulation, $CD39^+$ T_{RM} cells produced interferon-γ (IFN-γ), tumor necrosis factor-α (TNF-α), and interleukin-2 (IL-2) to a lesser extent than $CD39^-$ T_{RM} or non-T_{RM} cells (Fig. 10). Analysis of the polyfunctionality index(39), which scores the ability to simultaneously produce multiple cytokines, yielded similar results, confirming that $CD39^+$ T_{RM} cells are functionally exhausted.

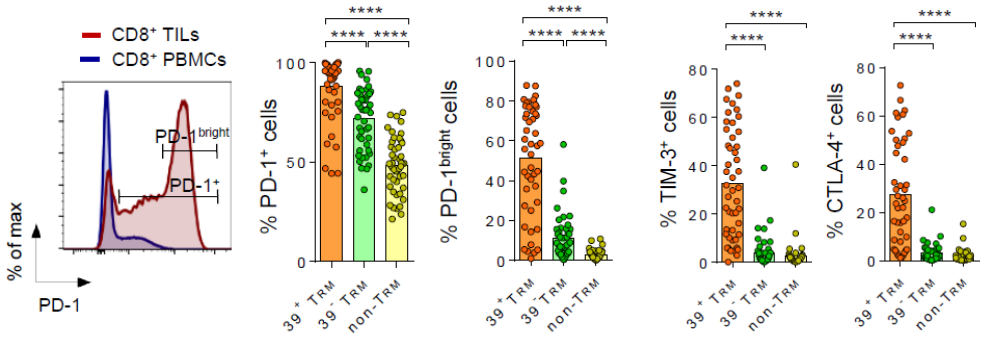

(a) (b)

Fig. 9. Representative flow cytometry plot of PD-1 expression on CD8+ T cell subpopulations in blood or tumors (a). PD-1bright is defined by higher expression of PD-1 on CD8+ T cells in tumors than the expression level of PD-1 on CD8+ T cells in blood. Frequencies of PD-1+ cells or PD-1bright cells among each fraction (n = 46). (b) Frequencies of TIM-3+ cells and CTLA-4+ cells among CD8+ T cell subpopulations in tumors (n = 46). Bars represent means. Two-sided unpaired Student's t test.

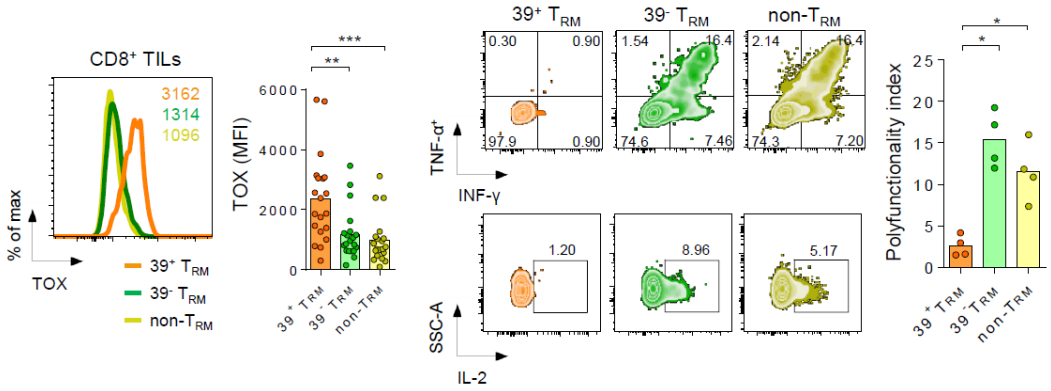

(a) (b) (c)

Fig. 10. (a) Representative flow cytometry plot of TOX expression (left) and the expression levels of TOX on $CD8^+$ T cell subpopulations in tumors (right, n = 20). Values inside the plot indicate the median fluorescence intensity (MFI) of TOX. Bars represent means. Two-sided unpaired Student's t test. Tumor lysates were stimulated with anti-CD3 antibody (1 μg/ml) for 6 hours and intracellular cytokine staining performed. Representative flow cytometry plots showing cytokine production by $CD8^+$ T cell subpopulations upon anti-CD3 stimulation (b). A polyfunctionality index was calculated using a formula that accounted for the combinatorial production of IFN-γ, TNF-α, and IL-2 (c, n = 4) (39). Bars represent means. Mann-Whitney test.

Next, we examined whether the characteristics of $CD39^+$ T_{RM} cells found in primary tumors are also observed in paired mLN tissues (Fig. 11). Tumor metastasis to LNs was confirmed by intraoperative frozen section examination. The frequencies of $CD39^+$ T_{RM} cells in primary tumors closely correlated with the frequencies of $CD39^+$ T_{RM} cells in paired mLN tissues. In addition, the transcriptional characteristics of mLN $CD39^+$ T_{RM} cells and tumor $CD39^+$ T_{RM} cells were similar to each other but distinct from $CD39^-$ T_{RM} cells and non-T_{RM} cells. Among $CD8^+$ T cells from mLNs, $CD39^+$ T_{RM} cells exhibited a significantly higher frequency of PD-1^+, TIM-3^+, and CTLA-4^+ cells than $CD39^-$ T_{RM} and non-T_{RM} cells (Fig.

12). In addition, anti-CD3-induced polyfunctionality was significantly reduced in CD39$^+$ T_{RM} cells compared to CD39$^-$ T_{RM} and non-T_{RM} cells among CD8$^+$ T cells from mLNs, confirming that CD39$^+$ T_{RM} cells in mLNs share a common feature with CD39$^+$ T_{RM} cells in primary tumors.

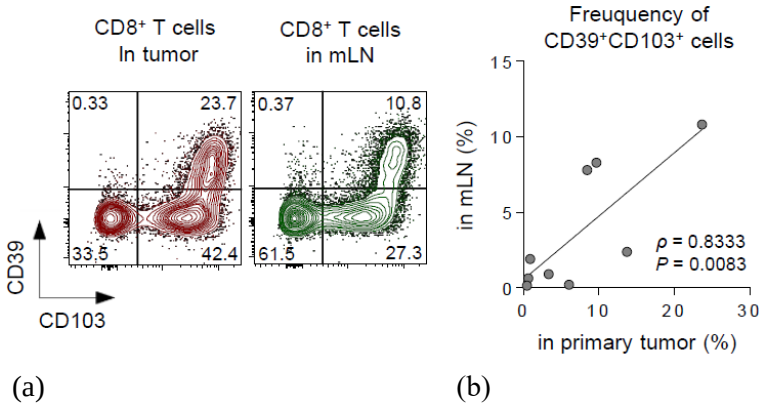

Fig. 11. Comparison of CD39 expression and CD103 expression on CD8$^+$ T cells between tumors and mLNs. (a) Representative flow cytometry plots from a patient. (b) Association of frequencies of CD39$^+$CD103$^+$ cells among CD8$^+$ T cells between primary tumors and paired mLNs (n = 9). ρ denotes Spearman correlation. P value obtained from two-sided t tests.

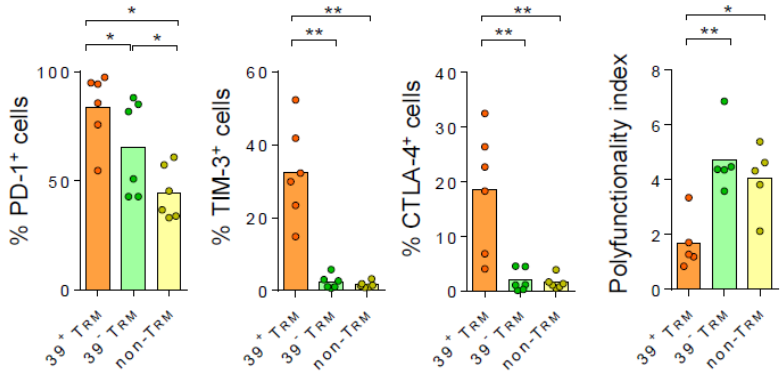

Fig. 12. (a) Frequencies of PD-1$^+$ cells, TIM-3$^+$ cells, and CTLA-4$^+$ cells in CD8$^+$ T cell

subpopulations in mLNs (n = 6). Bars represent means. Mann-Whitney test. (b) mLN lysates were stimulated with anti-CD3 antibody (1 μg/ml) for 6 hours and intracellular cytokine staining performed (n = 5). Bars represent means. Mann-Whitney test. *P ≤ 0.05, **P ≤ 0.01, ***P ≤ 0.001, and ****P ≤ 0.0001. SSC-A, side scatter area.

3. $CD39^+$ T_{RM} cells clonally overlap with other $CD8^+$ T-cell subpopulations within a compartment

To examine the clonality of $CD39^+$ TRM cells, we performed TCR analysis. To comprehensively compare $CD8^+$ T cells among different compartments (i.e., primary tumors, mLNs, and peripheral blood), we sorted $CD8^+$ T cells into various $CD8^+$ T-cell subpopulations and performed RNA-based bulk TCR sequencing (TCR-seq). We defined $CD8^+$ T-cell subsets using CCR7 and CD45RA according to the standard classification of human $CD8^+$ T cells (40-42). $CD8^+$ T cells were primarily sorted into $CCR7^+CD45RA^+$ naïve (TN), $CCR7^+$CD45RA- central memory T (TCM), CCR7-CD45RA- effector memory T (TEM), and CCR7-$CD45RA^+$ terminally differentiated effector memory T (TEMRA) cells. In tumors and mLNs, TEM cells were the predominant population and $CD103^+$ TRM cells were largely detected in the TEM population (Fig. 13). Accordingly, we further sorted tumor or mLN TEM cells into $CD39^+$ TRM, CD39- TRM, and non-TRM cells (Fig. 14).

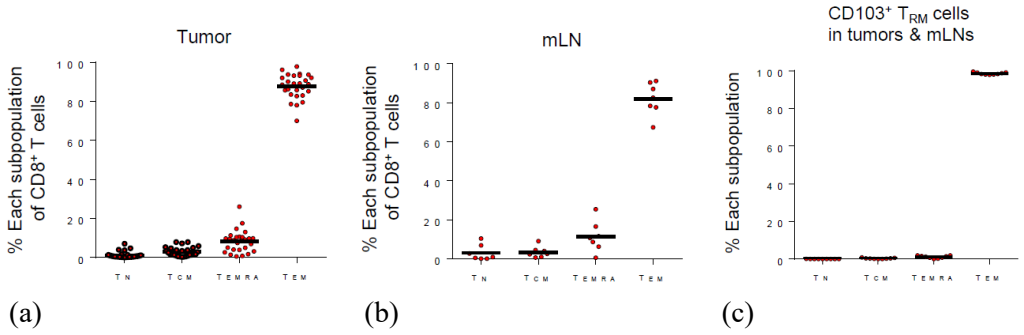

Fig. 13. Frequencies of each subpopulation among $CD8^+$ T cells in tumors (a) or mLNs (b). Frequencies of $CD103^+$ TRM cells among each $CD8^+$ T-cell subset in tumors and mLNs (N=9)(c). Bars represent means

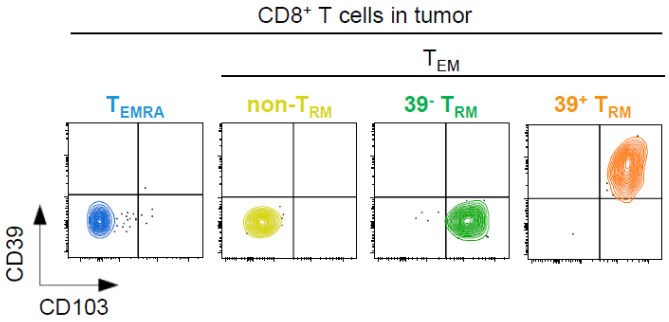

Fig. 14. Sorting strategy for $CD8^+$ T cells in tumors or mLNs for TCR-seq.

We analyzed the CDR3 sequences of the TCR-beta chains and found that $CD39^+$ TRM cells were not clonally distinct, but overlapped with other subpopulations within a compartment, such as tumors and mLNs, indicating that clonally identical $CD8^+$ T cells exhibit a heterogeneous differentiation status within tumors or mLNs (Fig. 15). Depending on the sample, >50% of $CD39^+$ TRM clonotypes, including high-rank clonotypes, overlapped with CD39- TRM or non-TRM clonotypes (Fig. 16).

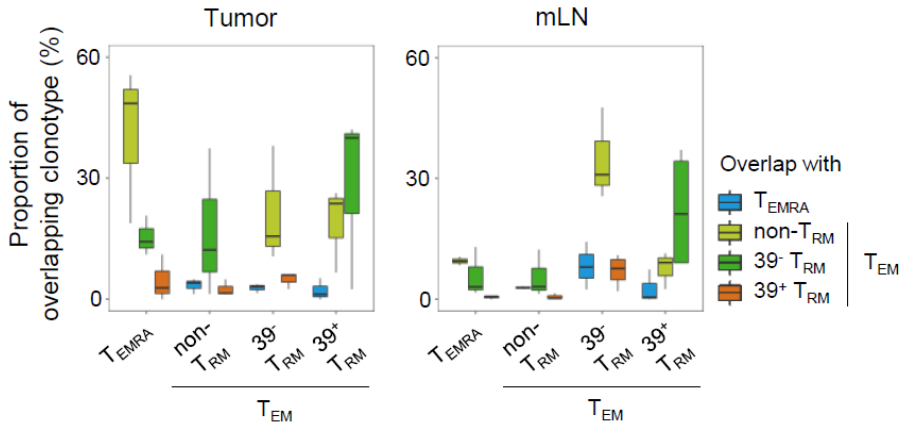

Fig. 15. Proportion of clonotypes in each CD8$^+$ T cell subpopulation that overlapped with other subpopulations in the same compartment: tumor (n = 3) and mLN (n = 4). Box plots show the median, box edges represent the first and third quartiles, and the whiskers extend to 1.5× the interquartile range.

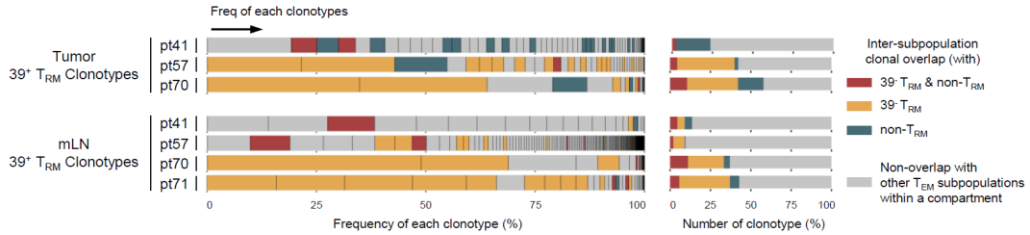

Fig. 16. Tumor CD39$^+$ TRM clonotypes (top) and mLN CD39$^+$ TRM clonotypes (bottom). Bar plots for each patient (left) show the frequencies of each clonotype among the total CD39$^+$ TRM clonotypes in each compartment. Each clonotype is colored according to the pattern of intersubpopulation clonal overlap. Bar plots for each patient (right) show the proportions of clonotypes by the pattern of inter-subpopulation clonal overlap.

Next, we examined whether a CD8$^+$ T cell clonal connection exists among different compartments. Investigation of the inter-compartmental overlap of CD8$^+$ T-cell clonotypes

showed that a considerable proportion (9% - 62%) of clonotypes from tumors or mLNs were also detected in other compartments (Fig. 17). Moreover, >80% of inter-compartmentally overlapping clonotypes were detected in the peripheral blood (Fig. 17), implying the presence of a $CD8^+$ T cell clonal connection between local tissue compartments and systemic blood. Inter-compartmental clonal overlaps between tissue compartments were largely observed between the same subpopulations of each compartment; for example, 6-49% of tumor $CD39^+$ TRM clonotypes overlapped with mLN $CD39^+$ TRM clonotypes. In addition, clonotypes of TEM cells in tumors or mLNs, including $CD39^+$ TRM, $CD39^-$ TRM, and non-TRM cells, mostly overlapped with TEM clonotypes in peripheral blood (Fig. 18). Overlapping $CD39^+$ TRM clonotypes between tumors and mLNs were frequently detected in blood TEM clonotypes, whereas non-overlapping $CD39^+$ TRM clonotypes were minor or undetectable in the blood (Fig. 19). Also, overlapping $CD39^-$ TRM or non-TRM clonotypes between tumors and mLNs were readily detected in blood TEM clonotypes, whereas non-overlapping CD39-TRM or non-TRM clonotypes were less detected in the blood. Taken together, these findings suggest a $CD8^+$ T cell clonal connection across different compartments, including local tissues and peripheral blood.

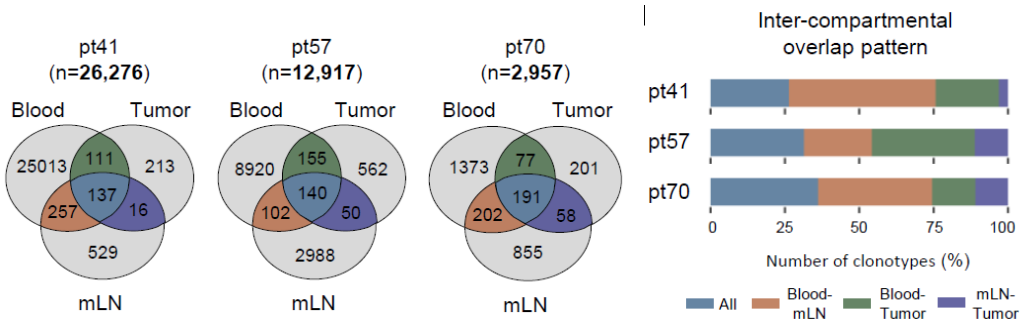

(a) (b)

Fig. 17. Venn diagram for each patient (a) showing the shared clonotypes across compartments. Values below patient numbers indicate the total number of unique clonotypes detected among all compartments for each patient. Values in the Venn diagram

indicate the numbers of unique clonotypes in each compartment or shared clonotypes among compartments in the overlapping regions. Bar plots for each patient (b) show the proportions of shared clonotypes among compartments by the pattern of inter-compartmental clonal overlap.

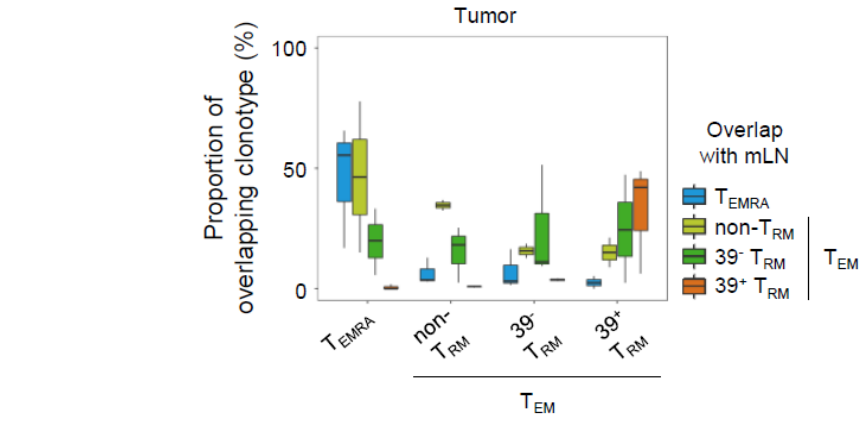

(a)

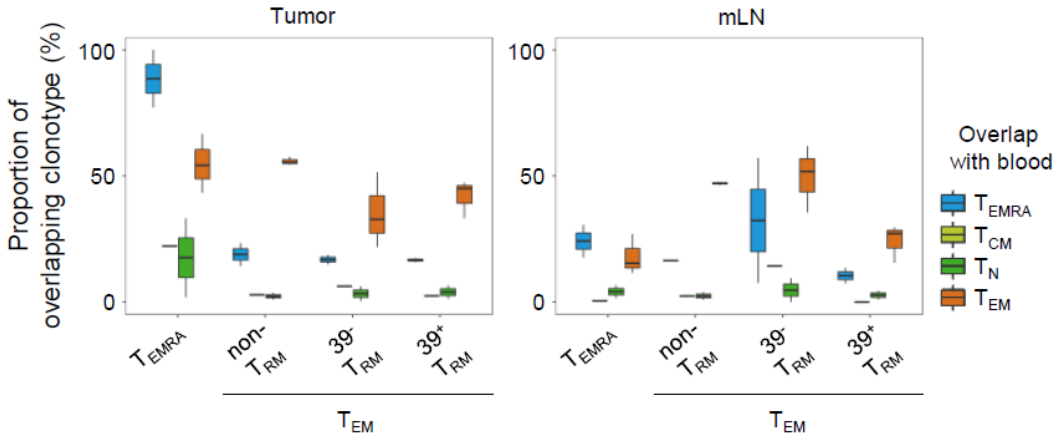

(b) (c)

Fig. 18. Proportion of clonotypes in each $CD8^+$ T cell subpopulation of tumors that overlapped with $CD8^+$ T cell subpopulations of mLNs (a, n = 3). Proportion of clonotypes in each $CD8^+$ T cell subpopulation of tumors (b, n = 3) and mLNs (c, n = 3) that overlapped

with CD8$^+$ T cell subpopulations in blood (lower). Box plots show the median, box edges represent the first and third quartiles, and the whiskers extend to 1.5× the interquartile range.

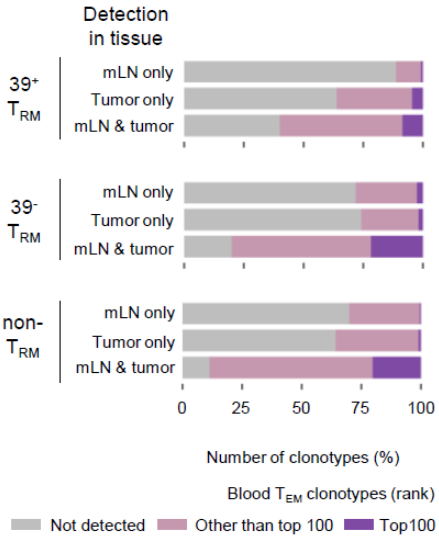

Fig. 19. Bar plots show proportions of tumor or mLN clonotypes by presence or rank in the TEM subpopulation in blood.

4. Tissue CD39$^+$ T_{RM} clonotypes with inter-subpopulational overlap are systemically connected with tumor reactivity

As described above, tumor or mLN CD39$^+$ T_{RM} cells clonally overlap with blood T_{EM} cells which do not include CD39$^+$ cells. We further analyzed the clonal connection between peripheral blood and tumors or mLNs. Large clonotypes in blood T_{EM} cells, such as the top 100 clonotypes, were detected in considerable counts in tissue compartments. We examined the subpopulation distribution of overlapping clonotypes in tumors and mLNs and found that both the top 100 and other blood T_{EM} clonotypes were distributed among various CD8$^+$ T-cell subpopulations in tumors and mLNs, including CD39$^-$ T_{RM} or CD39$^+$ T_{RM} cells, suggesting that blood T_{EM} cells may differentiate to CD39$^-$ T_{RM} or CD39$^+$ T_{RM} cells in

tumors and mLNs.

We further examined whether inter-subpopulationally overlapping clones in tumors or mLNs are readily detected in other compartments. We classified tumor CD39$^+$ T_{RM} clonotypes into inter-subpopulationally overlapping and non-overlapping clones and tracked these clones into other compartments. In particular, we analyzed the ranks of these clones in blood T_{EM} cells and the subpopulation distribution in mLNs. We also performed a similar analysis using mLN CD39$^+$ T_{RM} clonotypes (Fig. 20). Notably, tumor CD39$^+$ T_{RM} clonotypes with inter-subpopulation clonal overlap were more readily detected in blood T_{EM} cells as large clones than those without inter-subpopulation clonal overlap (Fig. 21). In addition, tumor CD39$^+$ T_{RM} clonotypes with inter-subpopulation clonal overlap were distributed among various subpopulations in mLNs, whereas those without inter-subpopulation clonal overlap had a restricted subpopulation distribution in mLNs. Similar results were observed in the analysis of mLN CD39$^+$ T_{RM} clonotypes with or without inter-subpopulation clonal overlap (Fig. 21). Tumor or mLN CD39$^+$ T_{RM} clonotypes with inter-subpopulation clonal overlap existed as CD39$^+$ T_{RM} clonotypes with inter-subpopulation clonal overlap in the other tissues. Given the tissue-resident property of T_{RM} cells, it can be inferred that blood T_{EM} cells undergo a differentiation process to CD39$^+$ T_{RM} cells in both tumors and mLNs.

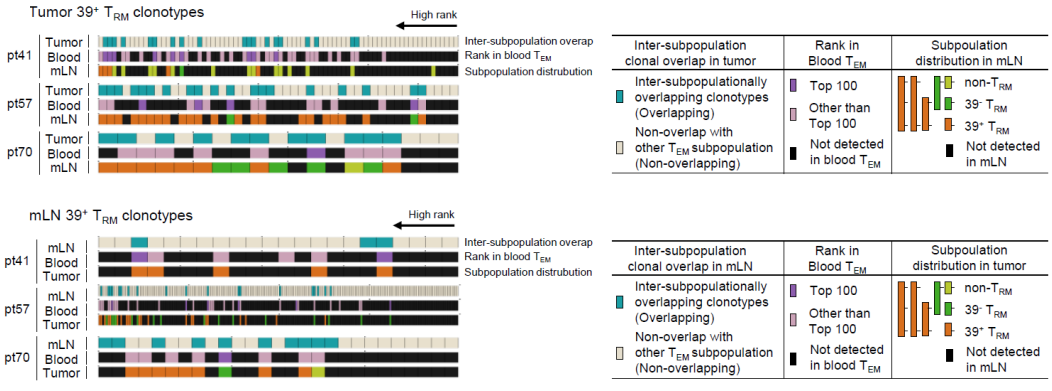

Fig. 20. Classification of tumor (upper) and mLN (lower) CD39$^+$ TRM clonotypes in

tumors, blood, and mLNs (right). Tumor CD39$^+$ TRM clonotypes were classified according to intersubpopulation clonal overlap in tumors, their presence or rank in blood TEM subpopulations, and their presence or subpopulation distribution in mLNs. Bar plots (left) show tumor CD39$^+$ TRM clonotypes arranged by their rank. In three bar plots for each patient, bars at the same position represent the classification of an identical clonotype in each compartment.

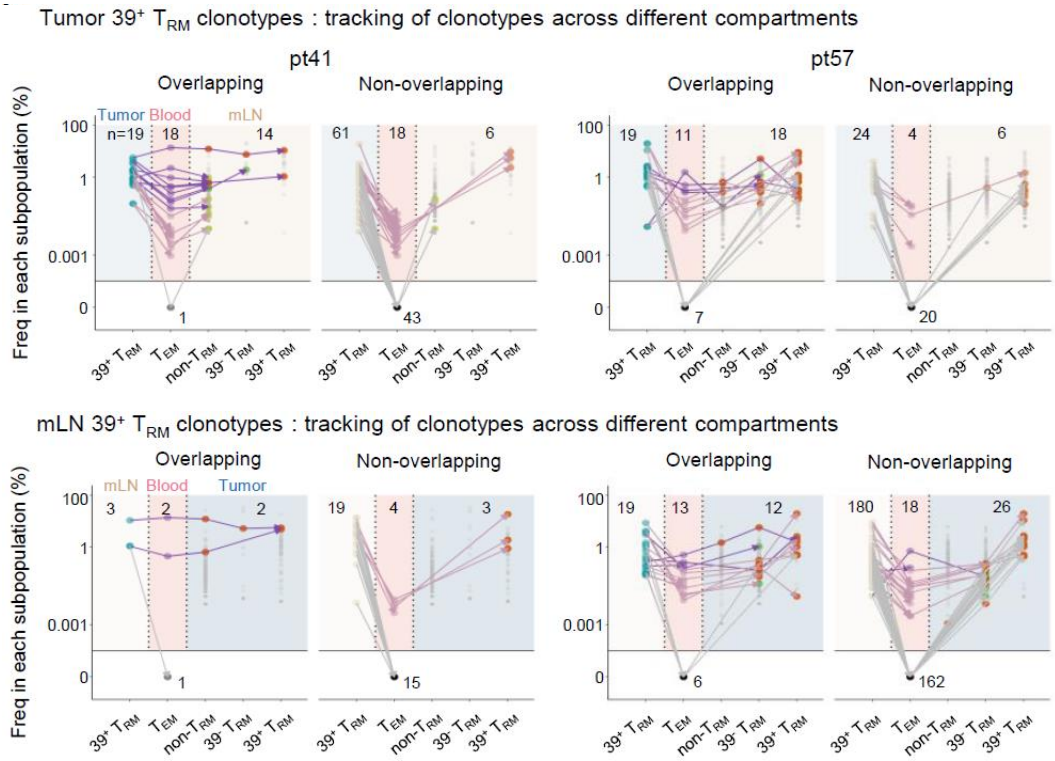

Fig. 21. Tracking of tumor CD39$^+$ TRM clonotypes or mLN CD39$^+$ TRM clonotypes across different compartments. Horizontal lines separate the absence and presence of clonotypes within a compartment. Values in the graph indicate the numbers of clonotypes detected in each compartment. Dots represent the frequencies of clonotypes and are colored by the classification of clonotypes in each subpopulation. Small gray dots in the graph indicate

the frequencies of total clonotypes in each subpopulation. Identical clonotypes are connected by lines, which are colored by their presence or rank in blood TEM subpopulations, across compartments.

Collectively, we concluded that tumor or mLN $CD39^+$ T_{RM} clones, especially with inter-subpopulation clonal overlap, are not compartmentalized, but systemically connected across blood and other tissues. Next, we asked whether $CD39^+$ T_{RM} cells recognize tumor antigens. To this end, we co-cultured sorted mLN $CD39^+$ T_{RM} cells with autologous $EPCAM^+$ cells sorted from tumor single-cell suspensions and examined the upregulation of 4-1BB, an activation-induced marker, to detect tumor-reactive $CD39^+$ T_{RM} cells. We found that the frequency of $4\text{-}1BB^+$ cells was increased by co-culturing with tumor $EPCAM^+$ cells (Fig. 22). We further sorted tumor-reactive $4\text{-}1BB^+CD39^+$ T_{RM} cells, performed TCR-seq analysis, and mapped $4\text{-}1BB^+CD39^+$ T_{RM} clonotypes to mLN $CD39^+$ T_{RM} clonotypes from the same patient (pt57). In a clonal tracking analysis, tumor-reactive $4\text{-}1BB^+CD39^+$ T_{RM} clonotypes with inter-subpopulation clonal overlap were readily detected in blood T_{EM} cells as large clones and broadly distributed among various subpopulations in tumors compared to those without inter-subpopulation clonal overlap (Fig. 22). This result demonstrates that tissue $CD39^+$ T_{RM} clonotypes include tumor antigen-specific TCR clones and are involved in systemically connected anti-tumor immune responses.

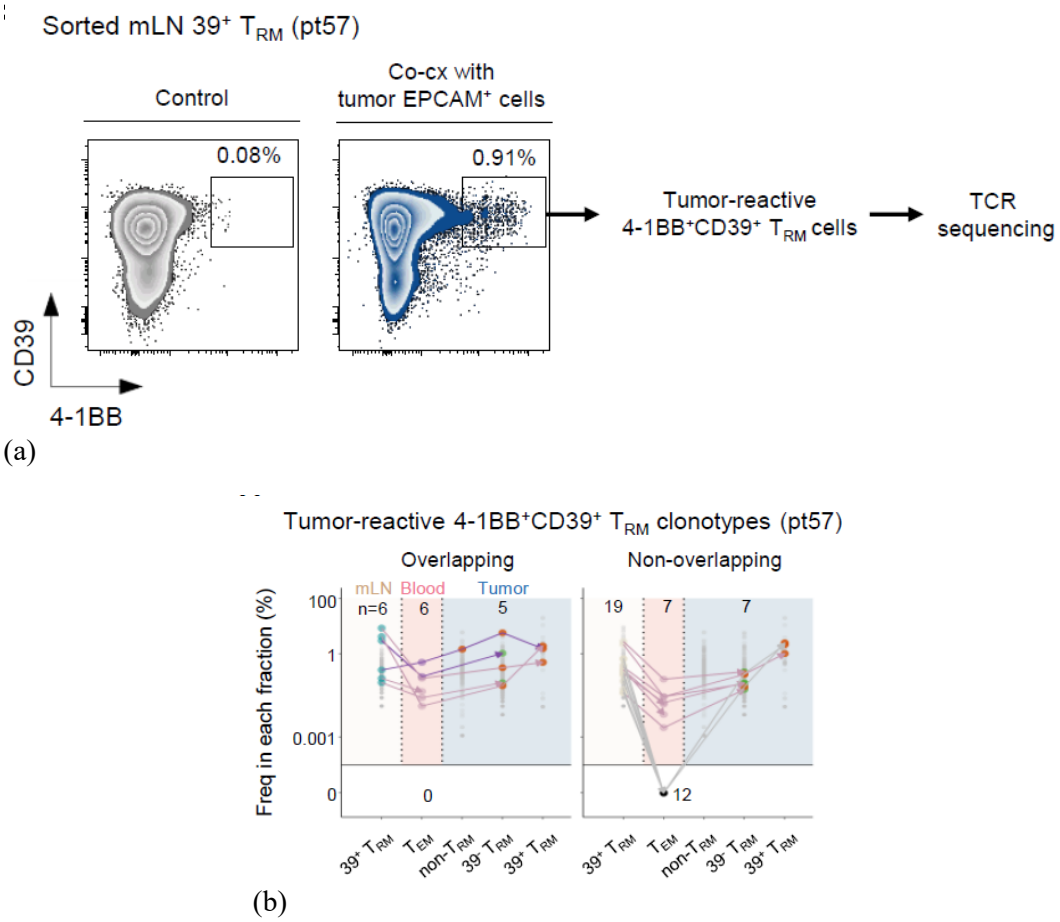

Fig. 22. Detection of CD39$^+$ TRM clonotypes reactive to autologous tumor cells (a). Fluorescence-activated cell sorting–sorted mLN CD39$^+$ TRM cells were cultured for expansion for 2weeks and then cocultured with autologous tumor EPCAM$^+$ cells. Tumor reactivity was confirmed by measuring 4-1BB$^+$ cells after coculture. Tumor-reactive clonotypes were obtained by TCR-seq of sorted 4-1BB$^+$CD39$^+$ TRM cells. Tumor-reactive 4-1BB$^+$CD39$^+$ TRM clonotypes were mapped to the mLN CD39$^+$ TRM clonotype from the identical patient (pt57) and tracked across different compartments (b).

5. The $CD39^+$ T_{RM} signature is enriched in TNBC and predicts patient survival

As tumor $CD39^+$ T_{RM} cells exhibit systemically connected clonotypes with tumor reactivity, we examined the enrichment of $CD39^+$ T_{RM} cells and the $CD39^+$ T_{RM} gene signature in tumor tissues among the molecular subtypes of early breast cancer, including $HR^+/HER\text{-}2^-$, $HER\text{-}2^+$, and TNBC (Fig. 23). Although the percentages of $CD8^+$ cells among $CD3^+$ TILs and $CD103^+$ T_{RM} cells among $CD8^+$ TILs were not significantly different for different subtypes, the percentage of $CD39^+$ T_{RM} cells among $CD8^+$ TILs was highest in TNBC tumors and lowest in $HR^+/HER\text{-}2^-$ tumors (Fig. 24). The frequencies of $CD39^+$ T_{RM} cells were not affected by other clinical characteristics, including tumor Ki-67 expression, neoadjuvant chemotherapy, pathological tumor stage, and LN metastasis. When we counted patients with >10% $CD39^+$ T_{RM} cells among $CD8^+$ TILs as $CD39^+$ T_{RM} cell-enriched cases, 36.4% of patients with TNBC were $CD39^+$ T_{RM} cell-enriched cases, whereas 6.7% and 14.8% of patients with $HR^+/HER\text{-}2^-$ and $HER\text{-}2^+$ were $CD39^+$ T_{RM} cell-enriched cases, respectively (Fig. 25). This result indicates that enrichment of $CD39^+$ T_{RM} cells in tumor tissues is qualitatively different among molecular subtypes of breast cancer, with the highest enrichment in TNBC.

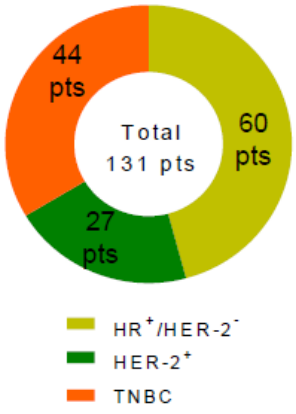

Fig. 23. Patient statistics according to molecular subtype of breast cancer (n = 131). pts, patients.

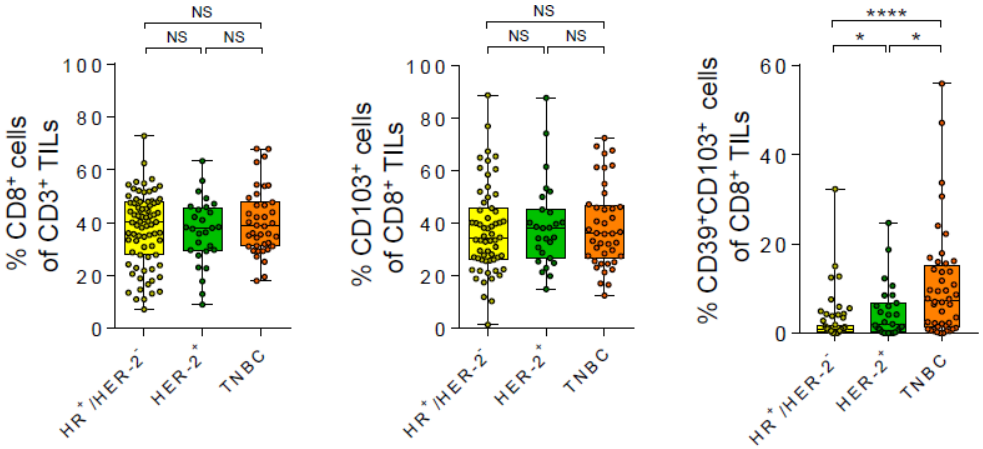

Fig. 24. Frequencies of $CD8^+$ T cells among $CD3^+$ TILs (a), $CD103^+$ cells among $CD8^+$ TILs (b), and $CD39^+CD103^+$ cells among $CD8^+$ TILs (c). Box plots show the median, box edges represent the first and third quartiles, and the whiskers extend to the minimum or maximum. Two-sided unpaired Student's t test.

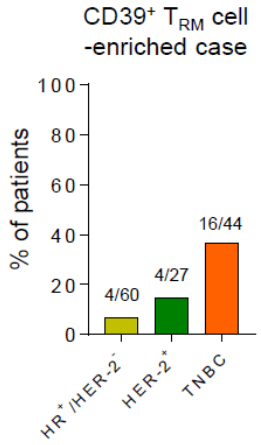

Fig. 25. Proportions of $CD39^+$ TRM cell–enriched cases, which were defined by >10% $CD39^+$ TRM cells among $CD8^+$ TILs in each subtype. The text above the bar indicates the number of $CD39^+$ TRM cell–enriched cases divided by the number of total patients.

To substantiate our findings in large independent cohorts, we extracted a gene set called the $CD39^+$ T_{RM} signature that comprised 48 genes that were significantly up-regulated in $CD39^+$ T_{RM} cells compared to $CD39^-$ T_{RM} cells from our bulk RNA-seq data and applied it to public datasets. Using gene expression data from the METABRIC consortium(43), we evaluated enrichment of the $CD39^+$ T_{RM} signature among normal breast tissue and primary breast tumors. Consistent with data from flow cytometry, enrichment scores for the $CD39^+$ T_{RM} signature in primary tumors were highest in TNBC tumors and lowest in HR^+/$HER\text{-}2^-$ tumors or normal breast tissue. These findings were recapitulated in an analysis using gene expression data from the TCGA dataset. Moreover, high enrichment of the $CD39^+$ T_{RM} signature in TNBC subtypes compared to HR^+/$HER\text{-}2^-$ subtypes was observed in a metastatic tissue cohort of breast cancer(44) (Fig. 26).

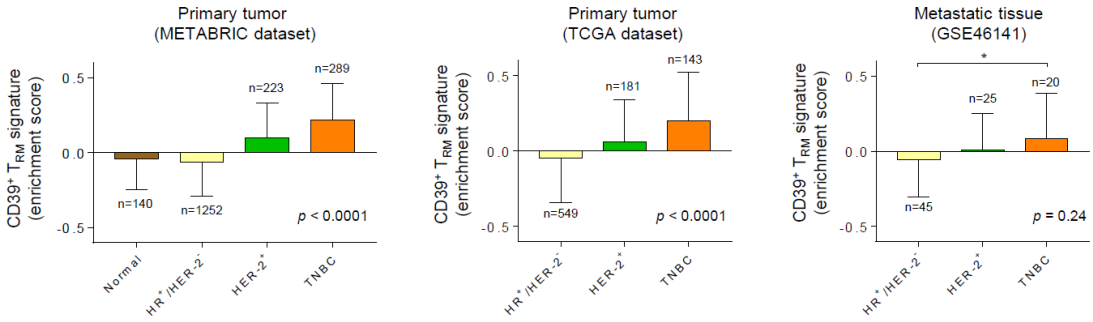

(a) (b) (c)

Fig. 26. Box plot showing the relative enrichment of the $CD39^+$ TRM signature in each subtype. Results were derived from the publicly available METABRIC (43) dataset for primary tumors (a, n = 1904), TCGA dataset for primary tumors (b, n = 873), and GSE46141 (44) dataset for metastatic tumors (c, n = 90). Box plots show the means and SD. Values above the box indicate the numbers of each subtype. Statistical analysis was performed by oneway ANOVA or two-sided unpaired Student's t test.

Next, we investigated whether the enrichment score for the $CD39^+$ T_{RM} signature in tumors

is associated with the survival of patients with breast cancer. To this end, we investigated the prognostic power of the $CD39^+$ T_{RM} signature using the METABRIC dataset of primary breast tumors. Among patients with $HR^+/HER\text{-}2^-$ or $HER\text{-}2^+$ tumors, cancer-specific survival was not different between patients with high and low scores for the $CD39^+$ T_{RM} signature (Fig. 27). However, among patients with TNBC subtypes, a high $CD39^+$ T_{RM} signature score had significantly better cancer-specific survival than a low $CD39^+$ T_{RM} signature score. Thus, enrichment of a $CD39^+$ T_{RM} feature that is different among molecular subtypes predicts the prognosis of patients with breast cancer, indicating that $CD39^+$ T_{RM} cells directly contribute to anti-tumor immune responses.

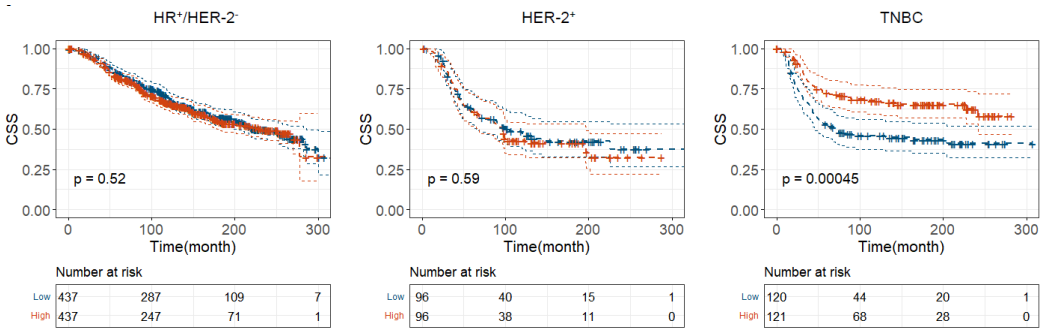

(a) (b) (c)

Fig. 27. Kaplan-Meier survival curves for cancer-specific survival among patients with $HR^+/HER\text{-}2-$ (a, n = 874), patients with $HER\text{-}2^+$ (b, n = 192), and patients with TNBC (c, n = 241) in the METABRIC dataset. Cases were stratified into two groups according to $CD39^+$ TRM signature enrichment. *P ≤ 0.05 and ****P ≤ 0.0001. CSS, cancer-specific survival.

6. $CD39^+$ T_{RM} cells are reinvigorated by blockade of PD-1 and CTLA-4 in vitro

Finally, we investigated whether tumor $CD39^+$ T_{RM} cells can be reinvigorated by the blockade of immune checkpoint receptors. We performed ex vivo functional assays of

CD8$^+$ TILs in the absence or presence of ICIs. We sorted CD8$^+$ TILs from a TNBC patient who was confirmed to have NY-ESO-1-specific CD8$^+$ TILs and stimulated them ex vivo with NY-ESO-1 overlapping peptides (OLPs) in the presence of autologous irradiated (3,000 rad) CD8-depleted tumor single-cell suspension. We confirmed PD-L1 expression on dendritic cells and macrophages in the tumor single-cell suspension. NY-ESO-1-induced proliferation of CD8$^+$ TILs was observed in CD39$^+$ T_{RM} cells (Fig. 28), supporting our previous finding that CD39$^+$ T_{RM} cells include tumor-reactive cells. Furthermore, anti-PD-1 with or without anti-CTLA-4 enhanced NY-ESO-1-induced proliferation of CD39$^+$ T_{RM} cells, but not CD39$^-$ T_{RM} or non-TRM cells. We also performed ex vivo proliferation assays by stimulating CD8$^+$ TILs from another TNBC patient with autologous tumor cells instead of NY-ESO-1 OLPs and obtained similar results (Fig. 28).

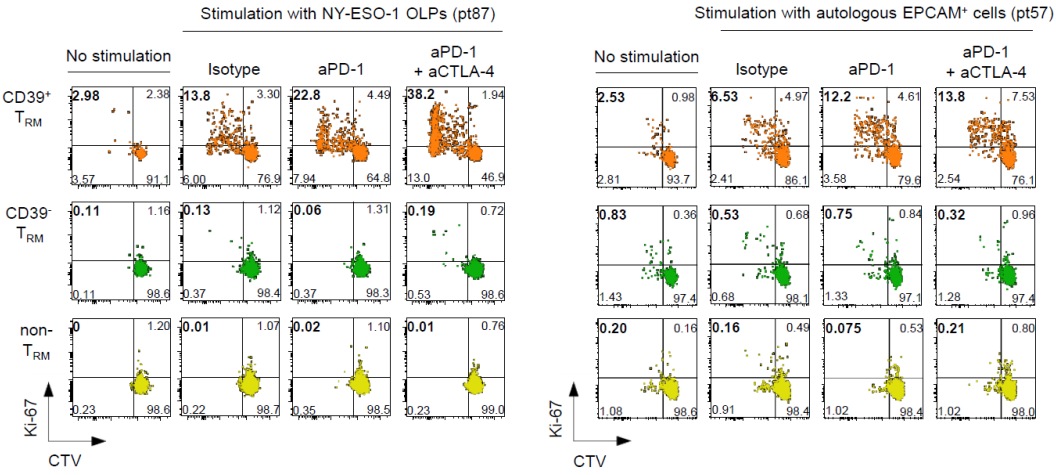

Fig. 28. Flow cytometry plots showing reinvigoration of CD39$^+$ TRM cells by ICIs. Sorted CD8$^+$ TILs from two TNBCs were stimulated in the presence of irradiated autologous feeder cells with NY-ESO-1 OLPs (a) or autologous EPCAM$^+$ tumor cells (b).

Next, we stimulated T cells with anti-CD3 in the absence or presence of ICIs using tumor

or mLN single-cell suspensions from various molecular subtypes and evaluated the functions of $CD8^+$ T cells, including the proliferation and production of IFN-γ and TNF-α. Both the cell proliferation and cytokine production of $CD8^+$ T cells were significantly increased by anti-PD-1 and further enhanced by combination with anti-CTLA-4 (Fig. 29/6, C and D). In further analysis, we examined the association between enrichment of $CD39^+$ T_{RM} cells and ICI-induced restoration of cytokine production. Two $HR^+/HER\text{-}2^-$ cases showed low frequencies of $CD39^+$ T_{RM} cells and limited restoration upon anti-PD-1 or anti-PD-1/anti-CTLA-4 treatment. However, $HER\text{-}2^+$ and TNBC cases exhibited broad-range distribution in both the frequency of $CD39^+$ T_{RM} cells and ICI-induced restoration of cytokine production. Overall, the restoration of IFN-γ and TNF-α production by anti-PD-1 or anti-PD-1/anti-CTLA-4 treatment significantly correlated with enrichment of $CD39^+$ T_{RM} cells (Fig. 30/6E). This result implies that $CD39^+$ T_{RM} cells have a capacity for functional restoration upon ICI treatment and may be an ICI-responding subpopulation.

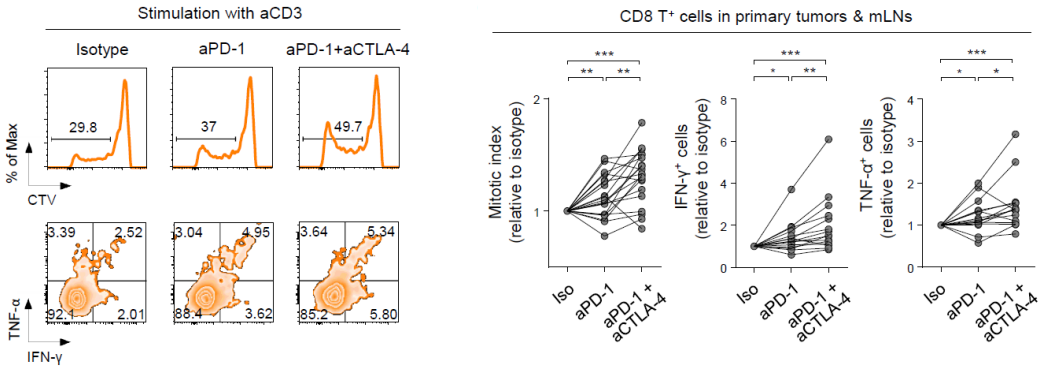

(a) (b)

Fig. 29. After culturing in the absence or presence of anti–PD-1 and/or anti–CTLA-4 for 144 hours, proliferation of each $CD8^+$ T cell subpopulationwas analyzed by CTV dilution and Ki-67 expression. The underlined values in bold represent the frequencies of proliferated $CD8^+$ T cells among each subpopulation. Tumor or mLN single cell suspensions from various molecular subtypes were stimulated with anti-CD3 antibodies in the absence or presence of anti–PD-1 and/or anti–CTLA-4. The proliferation of $CD8^+$ T

cells was analyzed by CTV dilution after 108 hours of culture (HER-2$^+$ tumors, n = 7; TNBC tumors, n = 10; TNBC mLNs, n = 3), and the cytokine production by CD8$^+$ T cells (HR$^+$/HER-2− tumors, n = 2; HER-2$^+$ tumors, n = 3; TNBC tumors, n = 7; TNBC mLNs, n = 3) was analyzed by intracellular staining of IFN-γ and TNF-α after 36 hours. Representative flow cytometry plots are presented in (a). (b) Data are presented as the fold change relative to isotype controls. The mitotic index was calculated as follows: total number of mitotic events divided by absolute number of precursor cells. Wilcoxon matched-pairs signed rank test.

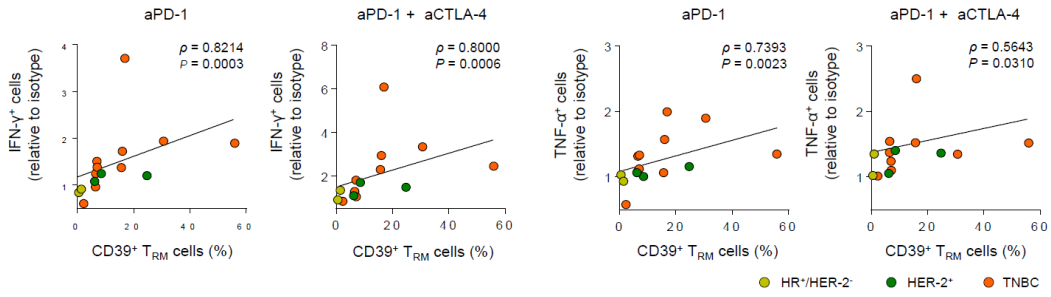

Fig. 30. Association between the frequencies of CD39$^+$ TRM cells among CD8$^+$ T cells and ICI-induced restoration of cytokine production.

To substantiate our in vitro findings in a clinical setting, we performed GSEA by applying a gene set obtained from a clinical trial of neoadjuvant anti-PD-1 treatment in breast cancer patients(*5*) to our bulk RNA-seq data. In this study, the single-cell transcriptomes of expanding versus non-expanding CD8$^+$ TILs were analyzed using pre-treatment tumors. Up-regulated genes in expanding CD8$^+$ TILs were significantly enriched in CD39$^+$ T_{RM} cells compared to CD39$^-$ T_{RM} cells (Fig. 31). We also examined our CD39$^+$ T_{RM} signature in a public scRNA-seq dataset obtained from a clinical trial of anti-PD-L1 treatment in patients with advanced TNBC(45). The single-cell transcriptomes were achieved from breast tumors or metastatic tumors from patients with TNBC treated with paclitaxel alone

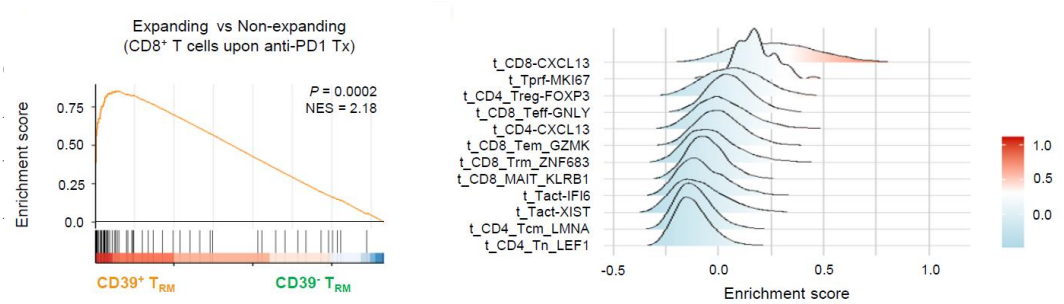

(a) (b)

Fig. 31. GSEA of up-regulated genes (a) in expanding versus nonexpanding $CD8^+$ T cells upon neoadjuvant anti–PD-1 treatment in $CD39^+$ TRM and CD39− TRM cells. The up-regulated gene set was derived from scRNA-seq analyses using pretreatment tumor samples from a clinical trial of neoadjuvant anti–PD-1 treatment in patients with breast cancer (5). Ridge plot (b) showing the enrichment score of our $CD39^+$ TRM signature genes in each T cell cluster of breast tumors. scRNA-seq data were obtained from a clinical trial of anti–PD-L1 treatment in patients with TNBC (45). ρ denotes Spearman correlation. P values were obtained from two-sided t tests. *P ≤ 0.05, **P ≤ 0.01, and ***P ≤ 0.001.

IV. DISCUSSION

In the current study, we report following findings: a) CD39 is expressed in a tumor-specific and exhausted T_{RM} subpopulation in both tumors and mLNs; b) $CD39^+$ T_{RM} cell clonotypes clonally overlap both in and across different compartments, implying their connection to systemic anti-tumor immunity; c) the $CD39^+$ T_{RM} signature is enriched in TNBC and predicts patient survival; and d) $CD39^+$ T_{RM} cells can be reinvigorated by ICIs and the restoration of $CD8^+$ T-cell effector functions by ICIs correlates with the relative frequency of $CD39^+$ T_{RM} cells.

Local anti-tumor immune responses in the tumor microenvironment have largely been investigated in tumor immunology(16, 46-48). However, local anti-tumor immune responses are not isolated from systemic and peripheral immunity(49-51). Thus, tracking $CD8^+$ T-cell clones across different compartments, including local tissues and peripheral blood, can provide new insights into understanding systemic anti-tumor immunity. Interestingly, $CD39^+$ T_{RM} cells in tumors or mLNs are not clonally distinct, but overlap with other $CD8^+$ T-cell subpopulations in the same compartment, revealing a differentiation process of $CD8^+$ T cells in tissues that is likely induced by encountering tumor antigens. In line with a recent finding that neoantigen-specific $CD8^+$ T cells are detected in both primary tumors and draining LNs in human NSCLC(52), $CD39^+$ T_{RM} cells were not only clonally connected, but also exhibited shared features between mLNs and primary tumors. In addition, tumor or mLN $CD39^+$ T_{RM} clonotypes, especially with inter-compartmental overlap, were readily detected in T_{EM} cells in the peripheral blood, where T_{RM} cells hardly exist. This finding suggests that blood T_{EM} cells undergo a differentiation process toward $CD39^+$ T_{RM} cells in both tumors and mLNs, requiring further studies. Furthermore, tumor $CD39^+$ T_{RM} clonotypes that have reactivity to autologous tumor cells were detected in blood and mLNs, implying that they do not only influence local anti-tumor immunity, but also have significance in systemic anti-tumor immunity.

Recent evidence from several types of human solid tumors indicates that bystander $CD8^+$ T cells that are specific to viral antigens are abundant in tumor tissues(16, 17, 52). However,

the presence of bystander $CD8^+$ TILs in breast cancer has not been investigated. In the current study, we detected CMV- and IAV-specific $CD8^+$ T cells in breast tumor tissues and peripheral blood and found that those in tumor tissues exhibit T_{RM} features. Proof-of-principle studies suggested that tumor-infiltrating $CD103^+$ T_{RM} cells localize in the proximity of breast tumor cells and are associated with a favorable prognosis in patients with TNBC (20, 21, 53). However, IAV-specific $CD8^+$ T cells in tumor also expressed CD103 and $CD103^+$ T_{RM} cells were detected in tumor-adjacent normal tissue to a similar extent with tumor tissue, implying that a further dissection of CD103 T_{RM} cells is needed for measurement of anti-tumor immune response in breast cancer. We found that most NY-ESO-1-specific $CD8^+$ TILs co-express CD39 and CD103, in contrast to virus-specific $CD8^+$ TILs, which lack CD39 expression. The proliferation of $CD8^+$ T cells responding to OLPs of NY-ESO-1 or autologous tumor cells was observed mostly in $CD39^+$ T_{RM} cells, further supporting their tumor-specific features. In line with tumor-specific features, $CD39^+$ T_{RM} cells in tumors or mLNs were dysfunctional cells with decreased cytokine production and reduced polyfunctionality. Also, CD39 T_{RM} signature, which is derived from bulk RNA-seq data comparing $CD39^+$ T_{RM} cells with $CD39^-$ T_{RM} cells, is related to better prognosis in TNBCs. Collectively, we confirmed that, in breast cancer, co-expression of CD39 and CD103 provided better understanding on the anti-tumor immune response elicited by $CD8^+$ T cells in tumors or mLNs than CD103 expression.

Patients with breast cancer have distinct risk profiles and pursue different treatment strategies according to molecular subtype(54). Previous studies have suggested the possibility of a different role of T cell-mediated anti-tumor immune responses among molecular subtypes(10-15). However, no studies have clearly demonstrated the differences in tumor-infiltrating $CD8^+$ T-cell characteristics among molecular subtypes. In this study, we showed that the enrichment levels of $CD39^+$ T_{RM} cells are significantly different among molecular subtypes. Particularly in HR^+/$HER\text{-}2^+$ subtypes, tumors included few $CD39^+$ T_{RM} cells and the enrichment level of the $CD39^+$ T_{RM} gene signature did not have prognostic value in predicting cancer-specific survival, suggesting a limited anti-tumor immune

response elicited by $CD8^+$ TILs. However, TNBC tumors contained considerable numbers of $CD39^+$ T_{RM} cells, which may be caused by higher immunogenicity compared to other subtypes and can be associated with previous observations of a better response to immunotherapy than other subtypes in clinical trials(55).

Neoadjuvant ICIs have been shown to enhance the anti-tumor immune response by eliciting a stronger and broader T-cell response compared to adjuvant ICIs in a mouse model or several types of human cancers(56-60). In addition, a single-cell analysis focusing on TCR showed that pre-existing T-cell clones in tumors can expand after neoadjuvant anti-PD-1 treatment in early breast cancer(5). Considering the known mechanism of ICIs, which reinvigorate tumor antigen-specific exhausted $CD8^+$ T cells, patient selection based on the enrichment level of $CD39^+$ T_{RM} cells in tumors could be optimal practice for implementing immunotherapy. In the present study, $CD39^+$ T_{RM} cells in tumors from early breast cancer patients responded to ICIs in vitro. Accordingly, active application of neoadjuvant ICIs could be considered in $CD39^+$ T_{RM} cell-enriched tumors. Because $CD39^+$ T_{RM} clonotypes are not only compartmentalized in tumors or mLNs, but also clonally connected to peripheral blood, neoadjuvant ICIs may enhance systemic anti-tumor immunity across multiple compartments. In our in vitro functional assays, combined blockade of CTLA-4 and PD-1 showed enhanced efficacy over the blockade of PD-1 alone, justifying the clinical application of combined CTLA-4 and PD-1/PD-L1 blockade for patients with $CD39^+$ T_{RM} cell-enriched breast cancer. In contrast, therapeutic strategies that stimulate antigen priming and tumor infiltration of tumor-specific T cells may precede ICI treatment in the case of $CD39^+$ T_{RM} cells-depleted tumors.

This study has some limitations. First, in the analysis of TCR clonal overlap, a sorted cell population can be contaminated by unwanted cells and, thus, minor clonotypes can potentially originate from contaminating cells. Although we confirmed that the effect of contaminating clonotypes was minimal, this issue should be considered with caution when interpreting our clonotype analysis. Second, our in vitro T-cell reinvigoration assays assessed the capacity of T cells for functional restoration in the presence of anti-PD-1 but

did not reflect the real in vivo responses to anti-PD-1 treatment. Further clinical studies are warranted among ICI-treated patients with breast cancer.

V. CONCLUSION

In summary, we dissected the heterogeneity of T_{RM} cells in terms of antigen specificity and found the $CD39^+$ T_{RM} subpopulation, which underlies a disparate role of the anti-tumor immune response among molecular subtypes of breast cancer. To the best of our knowledge, this is the first study tracking clonotypes of various $CD8^+$ T-cell subpopulations across multiple compartments, including tumors, mLNs, and blood, revealing the clonal connection of $CD39^+$ TRM cells with systemic anti-tumor immunity. Thus, the functional reinvigoration of $CD39^+$ TRM cells upon ICIs offers insights into the feasibility of neoadjuvant ICI treatment, particularly the combination of anti-PD-1/PD-L1 and anti-CTLA-4, in early breast cancer. Lastly, our findings have potential implications for different immuno-therapeutic strategies according to the enrichment level of $CD39^+$ TRM cells.

REFERENCES

1. P. Schmid, S. Adams, H. S. Rugo, A. Schneeweiss, C. H. Barrios, H. Iwata, V. Dieras, R. Hegg, S. A. Im, G. Shaw Wright, V. Henschel, L. Molinero, S. Y. Chui, R. Funke, A. Husain, E. P. Winer, S. Loi, L. A. Emens, I. M. T. Investigators, Atezolizumab and Nab-Paclitaxel in Advanced Triple-Negative Breast Cancer. N Engl J Med 379, 2108-2121 (2018).
2. T. Bachelot, T. Filleron, I. Bieche, M. Arnedos, M. Campone, F. Dalenc, F. Coussy, M. P. Sablin, M. Debled, C. Lefeuvre-Plesse, A. Goncalves, M. M. Reynier, W. Jacot, B. You, P. Barthelemy, B. Verret, N. Isambert, X. Tchiknavorian, C. Levy, J. C. Thery, T. L'Haridon, J. M. Ferrero, A. Mege, F. Del Piano, E. Rouleau, A. Tran-Dien, J. Adam, A. Lusque, M. Jimenez, A. Jacquet, I. Garberis, F. Andre, Durvalumab compared to maintenance chemotherapy in metastatic breast cancer: the randomized phase II SAFIR02-BREAST IMMUNO trial. Nat Med 27, 250-255 (2021).
3. P. Schmid, J. Cortes, L. Pusztai, H. McArthur, S. Kummel, J. Bergh, C. Denkert, Y. H. Park, R. Hui, N. Harbeck, M. Takahashi, T. Foukakis, P. A. Fasching, F. Cardoso, M. Untch, L. Jia, V. Karantza, J. Zhao, G. Aktan, R. Dent, J. O'Shaughnessy, K.-. Investigators, Pembrolizumab for Early Triple-Negative Breast Cancer. N Engl J Med 382, 810-821 (2020).
4. S. Loibl, M. Untch, N. Burchardi, J. Huober, B. V. Sinn, J. U. Blohmer, E. M. Grischke, J. Furlanetto, H. Tesch, C. Hanusch, K. Engels, M. Rezai, C. Jackisch, W. D. Schmitt, G. von Minckwitz, J. Thomalla, S. Kummel, B. Rautenberg, P. A. Fasching, K. Weber, K. Rhiem, C. Denkert, A. Schneeweiss, A randomised phase II study investigating durvalumab in addition to an anthracycline taxane-based neoadjuvant therapy in early triple-negative breast cancer: clinical results and biomarker analysis of GeparNuevo study. Ann Oncol 30, 1279-1288 (2019).
5. A. Bassez, H. Vos, L. Van Dyck, G. Floris, I. Arijs, C. Desmedt, B. Boeckx, M. Vanden Bempt, I. Nevelsteen, K. Lambein, K. Punie, P. Neven, A. D. Garg, H. Wildiers, J. Qian, A. Smeets, D. Lambrechts, A single-cell map of intratumoral changes during anti-PD1 treatment of patients with breast cancer. Nat Med 27, 820-832 (2021).
6. H. S. Rugo, J. P. Delord, S. A. Im, P. A. Ott, S. A. Piha-Paul, P. L. Bedard, J. Sachdev, C. Le Tourneau, E. M. J. van Brummelen, A. Varga, R. Salgado, S. Loi, S. Saraf, D. Pietrangelo, V. Karantza, A. R. Tan, Safety and Antitumor Activity of Pembrolizumab in Patients with Estrogen Receptor-Positive/Human Epidermal Growth Factor Receptor 2-Negative Advanced Breast Cancer. Clin Cancer Res 24, 2804-2811 (2018).
7. L. Wein, S. J. Luen, P. Savas, R. Salgado, S. Loi, Checkpoint blockade in the treatment of breast cancer: current status and future directions. Br J Cancer 119, 4-11 (2018).
8. E. Krasniqi, G. Barchiesi, L. Pizzuti, M. Mazzotta, A. Venuti, M. Maugeri-Sacca, G. Sanguineti, G. Massimiani, D. Sergi, S. Carpano, P. Marchetti, S. Tomao, T.

Gamucci, R. De Maria, F. Tomao, C. Natoli, N. Tinari, G. Ciliberto, M. Barba, P. Vici, Immunotherapy in HER2-positive breast cancer: state of the art and future perspectives. J Hematol Oncol 12, 111 (2019).

9. B. Vogelstein., N. Papadopoulos., V. E. Velculescu., S. Zhou., L. A. D. Jr., K. W. Kinzler., Cancer Genome Landscapes. Science 339, 1546-1558 (2013).
10. S. Luen, B. Virassamy, P. Savas, R. Salgado, S. Loi, The genomic landscape of breast cancer and its interaction with host immunity. Breast 29, 241-250 (2016).
11. S. E. Stanton, S. Adams, M. L. Disis, Variation in the Incidence and Magnitude of Tumor-Infiltrating Lymphocytes in Breast Cancer Subtypes: A Systematic Review. JAMA Oncol 2, 1354-1360 (2016).
12. S. Loi, N. Sirtaine, F. Piette, R. Salgado, G. Viale, F. Van Eenoo, G. Rouas, P. Francis, J. P. Crown, E. Hitre, E. de Azambuja, E. Quinaux, A. Di Leo, S. Michiels, M. J. Piccart, C. Sotiriou, Prognostic and predictive value of tumor-infiltrating lymphocytes in a phase III randomized adjuvant breast cancer trial in node-positive breast cancer comparing the addition of docetaxel to doxorubicin with doxorubicin-based chemotherapy: BIG 02-98. J Clin Oncol 31, 860-867 (2013).
13. S. Loi, S. Michiels, R. Salgado, N. Sirtaine, V. Jose, D. Fumagalli, P. L. Kellokumpu-Lehtinen, P. Bono, V. Kataja, C. Desmedt, M. J. Piccart, S. Loibl, C. Denkert, M. J. Smyth, H. Joensuu, C. Sotiriou, Tumor infiltrating lymphocytes are prognostic in triple negative breast cancer and predictive for trastuzumab benefit in early breast cancer: results from the FinHER trial. Ann Oncol 25, 1544-1550 (2014).
14. H. R. Ali, E. Provenzano, S. J. Dawson, F. M. Blows, B. Liu, M. Shah, H. M. Earl, C. J. Poole, L. Hiller, J. A. Dunn, S. J. Bowden, C. Twelves, J. M. Bartlett, S. M. Mahmoud, E. Rakha, I. O. Ellis, S. Liu, D. Gao, T. O. Nielsen, P. D. Pharoah, C. Caldas, Association between $CD8^+$ T-cell infiltration and breast cancer survival in 12,439 patients. Ann Oncol 25, 1536-1543 (2014).
15. C. Denkert, G. von Minckwitz, S. Darb-Esfahani, B. Lederer, B. I. Heppner, K. E. Weber, J. Budczies, J. Huober, F. Klauschen, J. Furlanetto, W. D. Schmitt, J.-U. Blohmer, T. Karn, B. M. Pfitzner, S. Kümmel, K. Engels, A. Schneeweiss, A. Hartmann, A. Noske, P. A. Fasching, C. Jackisch, M. van Mackelenbergh, P. Sinn, C. Schem, C. Hanusch, M. Untch, S. Loibl, Tumour-infiltrating lymphocytes and prognosis in different subtypes of breast cancer: a pooled analysis of 3771 patients treated with neoadjuvant therapy. The Lancet Oncology 19, 40-50 (2018).
16. W. Scheper, S. Kelderman, L. F. Fanchi, C. Linnemann, G. Bendle, M. A. J. de Rooij, C. Hirt, R. Mezzadra, M. Slagter, K. Dijkstra, R. J. C. Kluin, P. Snaebjornsson, K. Milne, B. H. Nelson, H. Zijlmans, G. Kenter, E. E. Voest, J. Haanen, T. N. Schumacher, Low and variable tumor reactivity of the intratumoral TCR repertoire in human cancers. Nat Med 25, 89-94 (2019).
17. Y. Simoni, E. Becht, M. Fehlings, C. Y. Loh, S. L. Koo, K. W. W. Teng, J. P. S. Yeong, R. Nahar, T. Zhang, H. Kared, K. Duan, N. Ang, M. Poidinger, Y. Y. Lee, A. Larbi, A. J. Khng, E. Tan, C. Fu, R. Mathew, M. Teo, W. T. Lim, C. K. Toh, B.

H. Ong, T. Koh, A. M. Hillmer, A. Takano, T. K. H. Lim, E. H. Tan, W. Zhai, D. S. W. Tan, I. B. Tan, E. W. Newell, Bystander CD8(+) T cells are abundant and phenotypically distinct in human tumour infiltrates. Nature 557, 575-579 (2018).

18. A. P. Ganesan, J. Clarke, O. Wood, E. M. Garrido-Martin, S. J. Chee, T. Mellows, D. Samaniego-Castruita, D. Singh, G. Seumois, A. Alzetani, E. Woo, P. S. Friedmann, E. V. King, G. J. Thomas, T. Sanchez-Elsner, P. Vijayanand, C. H. Ottensmeier, Tissue-resident memory features are linked to the magnitude of cytotoxic T cell responses in human lung cancer. Nat Immunol 18, 940-950 (2017).
19. J. R. Webb, K. Milne, P. Watson, R. J. Deleeuw, B. H. Nelson, Tumor-infiltrating lymphocytes expressing the tissue resident memory marker CD103 are associated with increased survival in high-grade serous ovarian cancer. Clin Cancer Res 20, 434-444 (2014).
20. P. Savas, B. Virassamy, C. Ye, A. Salim, C. P. Mintoff, F. Caramia, R. Salgado, D. J. Byrne, Z. L. Teo, S. Dushyanthen, A. Byrne, L. Wein, S. J. Luen, C. Poliness, S. S. Nightingale, A. S. Skandarajah, D. E. Gyorki, C. M. Thornton, P. A. Beavis, S. B. Fox, C. Kathleen Cuningham Foundation Consortium for Research into Familial Breast, P. K. Darcy, T. P. Speed, L. K. Mackay, P. J. Neeson, S. Loi, Single-cell profiling of breast cancer T cells reveals a tissue-resident memory subset associated with improved prognosis. Nat Med 24, 986-993 (2018).
21. C. A. Egelston, C. Avalos, T. Y. Tu, A. Rosario, R. Wang, S. Solomon, G. Srinivasan, M. S. Nelson, Y. Huang, M. H. Lim, D. L. Simons, T. F. He, J. H. Yim, L. Kruper, J. Mortimer, S. Yost, W. Guo, C. Ruel, P. H. Frankel, Y. Yuan, P. P. Lee, Resident memory $CD8^+$ T cells within cancer islands mediate survival in breast cancer patients. JCI Insight 4, (2019).
22. T. Duhen, R. Duhen, R. Montler, J. Moses, T. Moudgil, N. F. de Miranda, C. P. Goodall, T. C. Blair, B. A. Fox, J. E. McDermott, S. C. Chang, G. Grunkemeier, R. Leidner, R. B. Bell, A. D. Weinberg, Co-expression of CD39 and CD103 identifies tumor-reactive CD8 T cells in human solid tumors. Nat Commun 9, 2724 (2018).
23. C. M. Laumont, M. C. A. Wouters, J. Smazynski, N. S. Gierc, E. A. Chavez, L. C. Chong, S. Thornton, K. Milne, J. R. Webb, C. Steidl, B. H. Nelson, Single-cell Profiles and Prognostic Impact of Tumor-Infiltrating Lymphocytes Coexpressing CD39, CD103, and PD-1 in Ovarian Cancer. Clin Cancer Res 27, 4089-4100 (2021).
24. M. A. Eiva, D. K. Omran, J. A. Chacon, D. J. Powell, Jr., Systematic analysis of CD39, CD103, CD137, and PD-1 as biomarkers for naturally occurring tumor antigen-specific TILs. Eur J Immunol 52, 96-108 (2022).
25. G. Leem, J. Park, M. Jeon, E. S. Kim, S. W. Kim, Y. J. Lee, S. J. Choi, B. Choi, S. Park, Y. S. Ju, I. Jung, S. Kim, E. C. Shin, J. Y. Lee, S. H. Park, 4-1BB co-stimulation further enhances anti-PD-1-mediated reinvigoration of exhausted CD39(+) CD8 T cells from primary and metastatic sites of epithelial ovarian cancers. J Immunother Cancer 8, (2020).
26. F. P. Canale, M. C. Ramello, N. Núñez, C. L. Araujo Furlan, S. N. Bossio, M.

Gorosito Serrán, J. Tosello Boari, A. Del Castillo, M. Ledesma, C. Sedlik, E. Piaggio, A. Gruppi, E. A. Acosta Rodríguez, C. L. Montes, CD39 Expression Defines Cell Exhaustion in Tumor-Infiltrating CD8(+) T Cells. Cancer Res 78, 115-128 (2018).

27. P. K. Gupta, J. Godec, D. Wolski, E. Adland, K. Yates, K. E. Pauken, C. Cosgrove, C. Ledderose, W. G. Junger, S. C. Robson, E. J. Wherry, G. Alter, P. J. Goulder, P. Klenerman, A. H. Sharpe, G. M. Lauer, W. N. Haining, CD39 Expression Identifies Terminally Exhausted CD8+ T Cells. PLoS Pathog 11, e1005177 (2015).
28. B. C. Miller, D. R. Sen, R. Al Abosy, K. Bi, Y. V. Virkud, M. W. LaFleur, K. B. Yates, A. Lako, K. Felt, G. S. Naik, M. Manos, E. Gjini, J. R. Kuchroo, J. J. Ishizuka, J. L. Collier, G. K. Griffin, S. Maleri, D. E. Comstock, S. A. Weiss, F. D. Brown, A. Panda, M. D. Zimmer, R. T. Manguso, F. S. Hodi, S. J. Rodig, A. H. Sharpe, W. N. Haining, Subsets of exhausted CD8(+) T cells differentially mediate tumor control and respond to checkpoint blockade. Nat Immunol 20, 326-336 (2019).
29. Y. Qi, Y. Xia, Z. Lin, Y. Qu, Y. Qi, Y. Chen, Q. Zhou, H. Zeng, J. Wang, Y. Chang, Q. Bai, Y. Wang, Y. Zhu, L. Xu, L. Chen, Y. Kong, W. Zhang, B. Dai, L. Liu, J. Guo, J. Xu, Tumor-infiltrating CD39(+)CD8(+) T cells determine poor prognosis and immune evasion in clear cell renal cell carcinoma patients. Cancer Immunol Immunother 69, 1565-1576 (2020).
30. J. Yeong, L. Suteja, Y. Simoni, K. W. Lau, A. C. Tan, H. H. Li, S. Lim, J. H. Loh, F. Y. T. Wee, S. N. Nerurkar, A. Takano, E. H. Tan, T. K. H. Lim, E. W. Newell, D. S. W. Tan, Intratumoral CD39(+)CD8(+) T Cells Predict Response to Programmed Cell Death Protein-1 or Programmed Death Ligand-1 Blockade in Patients With NSCLC. J Thorac Oncol 16, 1349-1358 (2021).
31. M. Sade-Feldman, K. Yizhak, S. L. Bjorgaard, J. P. Ray, C. G. de Boer, R. W. Jenkins, D. J. Lieb, J. H. Chen, D. T. Frederick, M. Barzily-Rokni, S. S. Freeman, A. Reuben, P. J. Hoover, A. C. Villani, E. Ivanova, A. Portell, P. H. Lizotte, A. R. Aref, J. P. Eliane, M. R. Hammond, H. Vitzthum, S. M. Blackmon, B. Li, V. Gopalakrishnan, S. M. Reddy, Z. A. Cooper, C. P. Paweletz, D. A. Barbie, A. Stemmer-Rachamimov, K. T. Flaherty, J. A. Wargo, G. M. Boland, R. J. Sullivan, G. Getz, N. Hacohen, Defining T Cell States Associated with Response to Checkpoint Immunotherapy in Melanoma. Cell 176, 404 (2019).
32. F. O. Ademuyiwa, W. Bshara, K. Attwood, C. Morrison, S. B. Edge, A. R. Karpf, S. A. James, C. B. Ambrosone, T. L. O'Connor, E. G. Levine, A. Miliotto, E. Ritter, G. Ritter, S. Gnjatic, K. Odunsi, NY-ESO-1 cancer testis antigen demonstrates high immunogenicity in triple negative breast cancer. PLoS One 7, e38783 (2012).
33. A. Tessari, L. Pilla, D. Silvia, M. Duca, B. Paolini, M. L. Carcangiu, L. Mariani, F. G. de Braud, S. Cresta, Expression of NY-ESO-1, MAGE-A3, PRAME and WT1 in different subgroups of breast cancer: An indication to immunotherapy? Breast 42, 68-73 (2018).
34. O. Khan, J. R. Giles, S. McDonald, S. Manne, S. F. Ngiow, K. P. Patel, M. T. Werner,

A. C. Huang, K. A. Alexander, J. E. Wu, J. Attanasio, P. Yan, S. M. George, B. Bengsch, R. P. Staupe, G. Donahue, W. Xu, R. K. Amaravadi, X. Xu, G. C. Karakousis, T. C. Mitchell, L. M. Schuchter, J. Kaye, S. L. Berger, E. J. Wherry, TOX transcriptionally and epigenetically programs CD8($^{+}$) T cell exhaustion. Nature 571, 211-218 (2019).

35. A. C. Scott, F. Dundar, P. Zumbo, S. S. Chandran, C. A. Klebanoff, M. Shakiba, P. Trivedi, L. Menocal, H. Appleby, S. Camara, D. Zamarin, T. Walther, A. Snyder, M. R. Femia, E. A. Comen, H. Y. Wen, M. D. Hellmann, N. Anandasabapathy, Y. Liu, N. K. Altorki, P. Lauer, O. Levy, M. S. Glickman, J. Kaye, D. Betel, M. Philip, A. Schietinger, TOX is a critical regulator of tumour-specific T cell differentiation. Nature 571, 270-274 (2019).
36. C. Yao, H. W. Sun, N. E. Lacey, Y. Ji, E. A. Moseman, H. Y. Shih, E. F. Heuston, M. Kirby, S. Anderson, J. Cheng, O. Khan, R. Handon, J. Reilley, J. Fioravanti, J. Hu, S. Gossa, E. J. Wherry, L. Gattinoni, D. B. McGavern, J. J. O'Shea, P. L. Schwartzberg, T. Wu, Single-cell RNA-seq reveals TOX as a key regulator of CD8($^{+}$) T cell persistence in chronic infection. Nat Immunol 20, 890-901 (2019).
37. F. Alfei, K. Kanev, M. Hofmann, M. Wu, H. E. Ghoneim, P. Roelli, D. T. Utzschneider, M. von Hoesslin, J. G. Cullen, Y. Fan, V. Eisenberg, D. Wohlleber, K. Steiger, D. Merkler, M. Delorenzi, P. A. Knolle, C. J. Cohen, R. Thimme, B. Youngblood, D. Zehn, TOX reinforces the phenotype and longevity of exhausted T cells in chronic viral infection. Nature 571, 265-269 (2019).
38. E. J. Wherry, S. J. Ha, S. M. Kaech, W. N. Haining, S. Sarkar, V. Kalia, S. Subramaniam, J. N. Blattman, D. L. Barber, R. Ahmed, Molecular signature of CD8^{+} T cell exhaustion during chronic viral infection. Immunity 27, 670-684 (2007).
39. M. Larsen, D. Sauce, L. Arnaud, S. Fastenackels, V. Appay, G. Gorochov, Evaluating cellular polyfunctionality with a novel polyfunctionality index. PLoS One 7, e42403 (2012).
40. M. D. Martin, V. P. Badovinac, Defining Memory CD8 T Cell. Front Immunol 9, 2692 (2018).
41. F. Sallusto, D. Lenig, R. Förster, M. Lipp, A. Lanzavecchia, Two subsets of memory T lymphocytes with distinct homing potentials and effector functions. Nature 401, 708-712 (1999).
42. P. Romero, A. Zippelius, I. Kurth, M. J. Pittet, C. Touvrey, E. M. Iancu, P. Corthesy, E. Devevre, D. E. Speiser, N. Rufer, Four functionally distinct populations of human effector-memory CD8^{+} T lymphocytes. J Immunol 178, 4112-4119 (2007).
43. C. Curtis, S. P. Shah, S. F. Chin, G. Turashvili, O. M. Rueda, M. J. Dunning, D. Speed, A. G. Lynch, S. Samarajiwa, Y. Yuan, S. Graf, G. Ha, G. Haffari, A. Bashashati, R. Russell, S. McKinney, M. Group, A. Langerod, A. Green, E. Provenzano, G. Wishart, S. Pinder, P. Watson, F. Markowetz, L. Murphy, I. Ellis, A. Purushotham, A. L. Borresen-Dale, J. D. Brenton, S. Tavare, C. Caldas, S. Aparicio, The genomic and transcriptomic architecture of 2,000 breast tumours

reveals novel subgroups. Nature 486, 346-352 (2012).
44. S. Kimbung, A. Kovács, P. O. Bendahl, P. Malmström, M. Fernö, T. Hatschek, I. Hedenfalk, Claudin-2 is an independent negative prognostic factor in breast cancer and specifically predicts early liver recurrences. Mol Oncol 8, 119-128 (2014).
45. Y. Zhang, H. Chen, H. Mo, X. Hu, R. Gao, Y. Zhao, B. Liu, L. Niu, X. Sun, X. Yu, Y. Wang, Q. Chang, T. Gong, X. Guan, T. Hu, T. Qian, B. Xu, F. Ma, Z. Zhang, Z. Liu, Single-cell analyses reveal key immune cell subsets associated with response to PD-L1 blockade in triple-negative breast cancer. Cancer Cell, (2021).
46. M. Binnewies, E. W. Roberts, K. Kersten, V. Chan, D. F. Fearon, M. Merad, L. M. Coussens, D. I. Gabrilovich, S. Ostrand-Rosenberg, C. C. Hedrick, R. H. Vonderheide, M. J. Pittet, R. K. Jain, W. Zou, T. K. Howcroft, E. C. Woodhouse, R. A. Weinberg, M. F. Krummel, Understanding the tumor immune microenvironment (TIME) for effective therapy. Nat Med 24, 541-550 (2018).
47. W. Held, I. Siddiqui, K. Schaeuble, D. E. Speiser, Intratumoral CD8($^{+}$) T cells with stem cell-like properties: Implications for cancer immunotherapy. Sci Transl Med 11, (2019).
48. I. Siddiqui, K. Schaeuble, V. Chennupati, S. A. Fuertes Marraco, S. Calderon-Copete, D. Pais Ferreira, S. J. Carmona, L. Scarpellino, D. Gfeller, S. Pradervand, S. A. Luther, D. E. Speiser, W. Held, Intratumoral Tcf1($^{+}$)PD-1($^{+}$)CD8($^{+}$) T Cells with Stem-like Properties Promote Tumor Control in Response to Vaccination and Checkpoint Blockade Immunotherapy. Immunity 50, 195-211.e110 (2019).
49. K. J. Hiam-Galvez, B. M. Allen, M. H. Spitzer, Systemic immunity in cancer. Nat Rev Cancer 21, 345-359 (2021).
50. M. H. Spitzer, Y. Carmi, N. E. Reticker-Flynn, S. S. Kwek, D. Madhireddy, M. M. Martins, P. F. Gherardini, T. R. Prestwood, J. Chabon, S. C. Bendall, L. Fong, G. P. Nolan, E. G. Engleman, Systemic Immunity Is Required for Effective Cancer Immunotherapy. Cell 168, 487-502 e415 (2017).
51. A. K. Molodtsov, N. Khatwani, J. L. Vella, K. A. Lewis, Y. Zhao, J. Han, D. E. Sullivan, T. G. Searles, N. K. Preiss, T. B. Shabaneh, P. Zhang, A. R. Hawkes, B. T. Malik, F. W. t. Kolling, E. J. Usherwood, S. L. Wong, J. D. Phillips, K. Shirai, C. V. Angeles, S. Yan, T. J. Curiel, Y. H. Huang, C. Cheng, M. J. Turk, Resident memory CD8($^{+}$) T cells in regional lymph nodes mediate immunity to metastatic melanoma. Immunity 54, 2117-2132 e2117 (2021).
52. J. X. Caushi, J. Zhang, Z. Ji, A. Vaghasia, B. Zhang, E. H. Hsiue, B. J. Mog, W. Hou, S. Justesen, R. Blosser, A. Tam, V. Anagnostou, T. R. Cottrell, H. Guo, H. Y. Chan, D. Singh, S. Thapa, A. G. Dykema, P. Burman, B. Choudhury, L. Aparicio, L. S. Cheung, M. Lanis, Z. Belcaid, M. El Asmar, P. B. Illei, R. Wang, J. Meyers, K. Schuebel, A. Gupta, A. Skaist, S. Wheelan, J. Naidoo, K. A. Marrone, M. Brock, J. Ha, E. L. Bush, B. J. Park, M. Bott, D. R. Jones, J. E. Reuss, V. E. Velculescu, J. E. Chaft, K. W. Kinzler, S. Zhou, B. Vogelstein, J. M. Taube, M. D. Hellmann, J. R. Brahmer, T. Merghoub, P. M. Forde, S. Yegnasubramanian, H. Ji, D. M. Pardoll, K. N. Smith, Transcriptional programs of neoantigen-specific TIL in anti-PD-1-

treated lung cancers. Nature 596, 126-132 (2021).
53. Z. Q. Wang, K. Milne, H. Derocher, J. R. Webb, B. H. Nelson, P. H. Watson, CD103 and Intratumoral Immune Response in Breast Cancer. Clin Cancer Res 22, 6290-6297 (2016).
54. A. G. Waks, E. P. Winer, Breast Cancer Treatment. Jama 321, (2019).
55. S. Adams, M. E. Gatti-Mays, K. Kalinsky, L. A. Korde, E. Sharon, L. Amiri-Kordestani, H. Bear, H. L. McArthur, E. Frank, J. Perlmutter, D. B. Page, B. Vincent, J. F. Hayes, J. L. Gulley, J. K. Litton, G. N. Hortobagyi, S. Chia, I. Krop, J. White, J. Sparano, M. L. Disis, E. A. Mittendorf, Current Landscape of Immunotherapy in Breast Cancer: A Review. JAMA Oncol, (2019).
56. M. Chalabi, L. F. Fanchi, K. K. Dijkstra, J. G. Van den Berg, A. G. Aalbers, K. Sikorska, M. Lopez-Yurda, C. Grootscholten, G. L. Beets, P. Snaebjornsson, M. Maas, M. Mertz, V. Veninga, G. Bounova, A. Broeks, R. G. Beets-Tan, T. R. de Wijkerslooth, A. U. van Lent, H. A. Marsman, E. Nuijten, N. F. Kok, M. Kuiper, W. H. Verbeek, M. Kok, M. E. Van Leerdam, T. N. Schumacher, E. E. Voest, J. B. Haanen, Neoadjuvant immunotherapy leads to pathological responses in MMR-proficient and MMR-deficient early-stage colon cancers. Nat Med 26, 566-576 (2020).
57. C. U. Blank, E. A. Rozeman, L. F. Fanchi, K. Sikorska, B. van de Wiel, P. Kvistborg, O. Krijgsman, M. van den Braber, D. Philips, A. Broeks, J. V. van Thienen, H. A. Mallo, S. Adriaansz, S. Ter Meulen, L. M. Pronk, L. G. Grijpink-Ongering, A. Bruining, R. M. Gittelman, S. Warren, H. van Tinteren, D. S. Peeper, J. Haanen, A. C. J. van Akkooi, T. N. Schumacher, Neoadjuvant versus adjuvant ipilimumab plus nivolumab in macroscopic stage III melanoma. Nat Med 24, 1655-1661 (2018).
58. T. F. Cloughesy, A. Y. Mochizuki, J. R. Orpilla, W. Hugo, A. H. Lee, T. B. Davidson, A. C. Wang, B. M. Ellingson, J. A. Rytlewski, C. M. Sanders, E. S. Kawaguchi, L. Du, G. Li, W. H. Yong, S. C. Gaffey, A. L. Cohen, I. K. Mellinghoff, E. Q. Lee, D. A. Reardon, B. J. O'Brien, N. A. Butowski, P. L. Nghiemphu, J. L. Clarke, I. C. Arrillaga-Romany, H. Colman, T. J. Kaley, J. F. de Groot, L. M. Liau, P. Y. Wen, R. M. Prins, Neoadjuvant anti-PD-1 immunotherapy promotes a survival benefit with intratumoral and systemic immune responses in recurrent glioblastoma. Nature Medicine 25, 477-486 (2019).
59. T. Cascone, W. N. William, Jr., A. Weissferdt, C. H. Leung, H. Y. Lin, A. Pataer, M. C. B. Godoy, B. W. Carter, L. Federico, A. Reuben, M. A. W. Khan, H. Dejima, A. Francisco-Cruz, E. R. Parra, L. M. Solis, J. Fujimoto, H. T. Tran, N. Kalhor, F. V. Fossella, F. E. Mott, A. S. Tsao, G. Blumenschein, Jr., X. Le, J. Zhang, F. Skoulidis, J. M. Kurie, M. Altan, C. Lu, B. S. Glisson, L. A. Byers, Y. Y. Elamin, R. J. Mehran, D. C. Rice, G. L. Walsh, W. L. Hofstetter, J. A. Roth, M. B. Antonoff, H. Kadara, C. Haymaker, C. Bernatchez, N. J. Ajami, R. R. Jenq, P. Sharma, J. P. Allison, A. Futreal, J. A. Wargo, Wistuba, II, S. G. Swisher, J. J. Lee, D. L. Gibbons, A. A. Vaporciyan, J. V. Heymach, B. Sepesi, Neoadjuvant nivolumab or nivolumab plus ipilimumab in operable non-small cell lung cancer: the phase 2 randomized

NEOSTAR trial. Nat Med 27, 504-514 (2021).
60. J. Liu, S. J. Blake, M. C. Yong, H. Harjunpaa, S. F. Ngiow, K. Takeda, A. Young, J. S. O'Donnell, S. Allen, M. J. Smyth, M. W. Teng, Improved Efficacy of Neoadjuvant Compared to Adjuvant Immunotherapy to Eradicate Metastatic Disease. Cancer Discov 6, 1382-1399 (2016).
61. M. I. Love, W. Huber, S. Anders, Moderated estimation of fold change and dispersion for RNA-seq data with DESeq2. Genome Biol 15, 550 (2014).
62. J. Gao, B. A. Aksoy, U. Dogrusoz, G. Dresdner, B. Gross, S. O. Sumer, Y. Sun, A. Jacobsen, R. Sinha, E. Larsson, E. Cerami, C. Sander, N. Schultz, Integrative analysis of complex cancer genomics and clinical profiles using the cBioPortal. Sci Signal 6, pl1 (2013).
63. T. Barrett, S. E. Wilhite, P. Ledoux, C. Evangelista, I. F. Kim, M. Tomashevsky, K. A. Marshall, K. H. Phillippy, P. M. Sherman, M. Holko, A. Yefanov, H. Lee, N. Zhang, C. L. Robertson, N. Serova, S. Davis, A. Soboleva, NCBI GEO: archive for functional genomics data sets--update. Nucleic Acids Res 41, D991-995 (2013).
64. D. A. Bolotin, S. Poslavsky, I. Mitrophanov, M. Shugay, I. Z. Mamedov, E. V. Putintseva, D. M. Chudakov, MiXCR: software for comprehensive adaptive immunity profiling. Nat Methods 12, 380-381 (2015).
65. C. E. Shannon, The mathematical theory of communication. 1963. MD Comput 14, 306-317 (1997).
66. V. I. Nazarov, M. V. Pogorelyy, E. A. Komech, I. V. Zvyagin, D. A. Bolotin, M. Shugay, D. M. Chudakov, Y. B. Lebedev, I. Z. Mamedov, tcR: an R package for T cell receptor repertoire advanced data analysis. BMC Bioinformatics 16, 175 (2015).
67. M. Morisita, Measuring of the dispersion of individuals and analysis of the distributional patterns. Mem. Fac. Sci. Kyushu Univ., Ser. E (Biol.) 2, 215-235 (1959).

ABSTRACT(IN KOREAN)

CD39$^+$ 조직 상주 기억 CD8$^+$ T 세포는 유방암에서 항종양 면역 반응을 매개한다

<지도교수 김승일>

연세대학교 대학원 의학과

김 지 예

면역 관문 억제제는 유방암 표준 치료의 하나로 자리 잡았으나, 일부 환자군에서만 그 효과를 보이고 있다. 유방암에서 항종양 면역 반응을 더 잘 이해하기 위해, 본 연구에서는 수술 받는 131명의 조기 유방암 환자로부터 구득한 유방암 조직, 전이가 확인 된 액와 림프절 그리고 말초 혈액으로부터 CD8$^+$ T 세포의 이질성을 탐색하고자 하였다. CD8$^+$ 조직 상주 기억 T 세포에는 유방암 비특이적인 바이러스 특이 CD8$^+$ T 세포와 유방암 특이적인 CD8$^+$ T 세포가 모두 존재하였고, 이 중 CD39 발현은 유방암 및 전이성 액와 림프절 모두에서 종양 특이적이고 기능적으로 탈진한 세포군에서 관찰되었다. CD39$^+$ 조직 상주 기억 세포의 클로노타입은 동일 구역 내의 CD8$^+$ T 세포 소집단 클로노타입 및 서로 다른 구역의 클로노타입과 공통된 부분을 보여주었고, 이는 CD39$^+$ 조직 상주 기억 세포가 항종양 면역 반응에 전신적으로 연결되어 있음을 시사한다. 또한, CD39$^+$ 조직 상주 기억 세포의 발현 빈도는 유방암의 아형에 따라 다르게 분포하였고 삼중 음성 유방암에서 그 빈도가 가장 높았다. 생체 외 실험에서 유방암 혹은 전이성 액와 림프절의 CD8$^+$ T 세포는 PD-1 과 동시에 혹은 따로 CTLA-4 항체를 처리 하였을 때, CD39$^+$ 조직 상주 기억 T 세포의 존재 하에서 그 분열과 사이토카인 생성이 회복됨을 확인하였다. 결론적으로, CD39$^+$ 조직 상주 기억 세포는 면역 관문

억제제 치료에 대한 기능 회복에 중요한 역할을 하며, 항종양 면역 반응의 매개체로 작용할 것으로 생각된다.

핵심되는 말 : 유방암, $CD39^+$ 조직 상주 기억 $CD8^+$ T 세포, 항종양 면역 반응